

EVALUATING POSSIBLE ERRORS IN IMU SENSORS

Çağın AĞIRDEMİR

Dr. Serdar ARITAN

Supervisor

SUBMITTED IN FULFILMENT OF THE REQUIREMENTS FOR THE
DEGREE OF
MASTER OF SCIENCE

INSTITUTIE OF INFORMATICS
DEPARTMENT OF COMPUTER GRAPHICS



2022

ABSTRACT

EVALUATING POSSIBLE ERRORS IN IMU SENSORS

Cağın AĞIRDEMİR

Master, Department of Computer Graphics

Supervisor: Dr. Serdar ARITAN

September 2022

Sensors with inertial working principle are used in many different fields, especially in human modeling and navigation applications. Accelerometer and gyroscope sensors, which are the main components of inertial sensors, can be produced with micromechanical systems technology today. A decrease is observed in their performance as well as low cost and high production amount facts. Therefore, various error compensation algorithms have been proposed to improve inertial sensor performances. Deterministic and probabilistic inertial sensor errors and their relationships with the parameters that cause these errors from the basis of error compensation algorithms In order for error compensation algorithms to perform high accuracy error compensation, it is critical to establish error modeling that reveals the relationship between sensor errors and error sources. In this thesis, a test device capable of simulating human arm and leg movements was produced in order to model inertial sensor errors. Three different axes of inertial sensors at two different angular velocities were applied separately with a human motion simulation test device, and sensor error distributions were calculated using the Gaussian distribution model. The effect of angular motion physical effects and stability of sensor temperature on inertial sensor error distributions was investigated using the test device.

Keywords: IMU, Modelling, Motion Capture Systems, MEMS

CONTENTS

Abstract	2
Declaration	5
Abbreviations	6
1.Introduction	7
2.Pre-studies to Error Modelling in Inertial Sensor	9
3.Method	12
3.1. Determining Motor Type	12
3.2. Determining Inertial Sensor	13
3.3. Design of Experimental Setup	14
3.3.1. Produced Components	16
3.3.1.1. Tray Component	16
3.3.1.2. Battery Holder	17
3.3.1.3. Marker Holder	17
3.3.2. Motor Control System	18
3.4. Calibration and Precision Test for Optical System	19
3.5. Data Acquisition System	22
3.5.1. Raspberry Pi Configuration	22
3.5.2. IMU Configuration	22
3.5.3. Data Acquisition Software	23
3.6. IMU Deterministic Error Modelling	23
3.6.1. Acceleration and Gyroscope Bias Errors	25
3.6.2. Acceleration Scale Factor and Misalignment Errors	26
3.7. Angular Movement Experiment Procedures	26
4.Findings	28
4.1. Device Vibration Findings	28
4.2. Sensor Temperature Findings	29

4.3. 45 Degree/Second Experiment Findings	30
4.3.1. Rotation in X-Axis Findings	30
4.3.2. Rotation in Y-Axis Findings	32
4.3.3. Rotation in Z-Axis Findings	34
4.4. 180 Degree/Second Experiment Findings	36
4.4.1. Rotation in X-Axis Findings	36
4.4.2. Rotation in Y-Axis Findings	38
4.4.3. Rotation in Z-Axis Findings	40
5.Discussion	42
6.Results	44
7.References	45

Declaration

I declare that, except where explicit reference is made to the contribution of others, that this dissertation is the result of my own work and has not been submitted for any other degree at the Hacettepe University or any other institution.

Çağın AĞIRDEMİR

22.09.2022

Abbreviations

IMU	Inertial Measurement Unit
MEMS	Micromechanical Systems
ODR	Output Data Rate
DoF	Degree of Freedom
PMU	Power Management Unit
ARM	Advanced RISC Machines
I2C	Inter-Integrated Circuit
SSH	Secure Shell
IP	Internet Protocol
RAM	Random Access Memory
UART	Universal Asynchronous Receiver/Transmitter
FIFO	First In First Out
GPS	Global Position System
DC	Direct Current

1. INTRODUCTION

Human movement simulation is transmitting from real-world movements to computer environment. Simulation process can be proceeded by placing the equipment on the person to be modeled. The simulated data can be used in variety field. One of them is humanoid robot studies. Animatronics can be shown as an example of humanoid robotics. Animatronics are mechanic robot puppet and different type of automaton. They are often used in movies, theme parks and to depict cartoon or game characters in attraction centers. One of the major problems of the humanoid robots is to provide that robot movements are humanoid. One of solutions for this problem is to convey movements from human to robots through human movement.

Another field which used human movement simulation is medical studies. For examples, scientist can measure effects of treatments which applied on the patient who has gait disorder by evaluating human modelling simulation data. But equipment to acquisition human movement simulation data that is not available in every clinic for economic issues [3]. Human movement simulation used in other fields such as sports, military and video game and animation studies besides medical studies and humanoid robots.

A motion capture system is needed for human motion simulation. Motion capture systems can be based on 3 different working principles. These principles can specify as optic, electromagnetic and inertial [1]. These systems based on different working principles has advantages and disadvantages than each other's like precision, working area limitation and hardware costs. Motion capture system which based on inertial working principles is used IMU sensors. IMU sensors stand out with facts like costs, easily carried and able to fast-implementations. Besides these advantage specs, IMU sensors has many errors due to their hardware structure. Sensors errors can be divided into two categories that are deterministic and random [10]. Deterministic error can be determined through tests which applied before the usage. But random error cannot be determined due to occur in runtime. Sensor outcomes especially position calculations getting worst due to calculate

cumulatively. As a result of this errors, position calculations be unreliable rapidly. As if random errors compensated completely, IMU sensors has white noises. Therefore, IMU sensors outcomes have to correction through aiding system.

When searching academic studies databases and IEEE (Institute of Electrical and Electronics Engineers) academic search engine, it is seen that there are few open-source algorithms. However, there are many importing advances at commercial applications. Market research by Fortune Business Insights company show that measures systems used IMU sensors market size 17 billion United State Dollars in 2019 and will reach 24 billion United States Dollars in 2027 [6]. Academic outputs and open-sources methods are less than commercial one's situation is the main motivation source for this thesis.

The main purpose in scope of this thesis is to improve navigation calculation in IMU sensors by modelling possible errors in IMU sensors during stable angular movements which angular rates determined in light of human arm and leg angular movement limits. Firstly, deterministic error was detected using static tests to reach this purpose. A experimental device was needed to apply the angular motion simulation of the human leg and arm to the sensor in 2D. Commercial test devices, flight movement simulators and industrial robot arms are reviewed. As result of, to manufacture a turn-table test device that low-cost, reliable and it has high control capability is decided. The device calibrated by using an optic system capable to measure position in specific area precisely.

2. PRE-STUDIES TO ERROR MODELLING IN IMU SENSORS

MEMS IMU sensors often preferred as human capture systems due to some facts such as low battery usage, minimal size and no limitation other than battery life. With the decrease in the production costs of the gyroscope and accelerometer sensor, which constitute the inertial measurement unit, an increase has occurred in the production quantities. As the sensors produced as MEMS are produced in high numbers and at low costs, a decrease in sensor performance is observed. The use of MEMS inertial sensors in combination with a complementary sensor or sensors and error compensation algorithms becomes imperative to obtain a reliable navigation calculation. To integrate a complementary sensor and a MEMS inertial sensor, understanding the characteristics of the different error sources and the random variation of these error is of great importance in order to provide a continuous and reliable navigation calculation [20]. In this point, some navigation experiments were carried out with the Madgwick AHRS complementary filter (Figure 2.1).

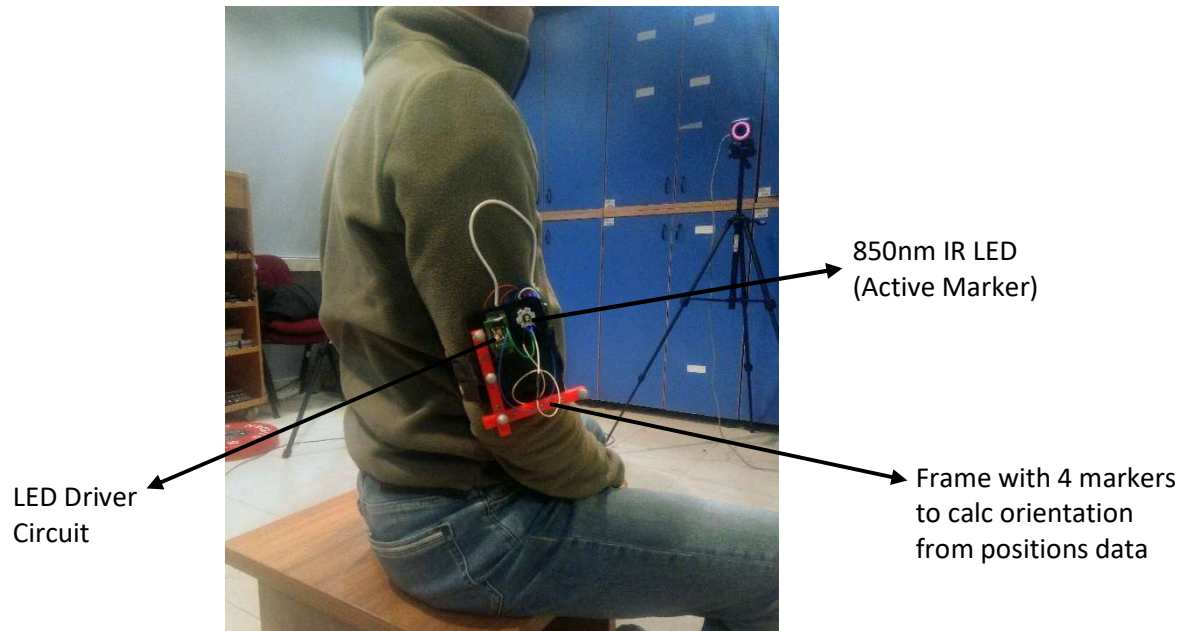


Figure 2.1: Pre-studies experiments

After pre-study experiments, it was realized that just complementary filters were not sufficient for reliable inertial navigation. Therefore, the focus is on modeling sensor errors and predictive filters in this thesis. Inertial sensors have 2 types of errors as deterministic errors and random errors [18]. Random errors include bias shifts or scale factor error, and rate which these errors change with time [21]. Random errors must be modeled stochastically. Deterministic sources of error include bias and scale factor errors that can be eliminated with certain calibration procedures in a laboratory setting [8]. Deterministic errors are an important part of IMU errors. Therefore, the design of deterministic error estimation and compensation algorithms is more important than stochastic error compensation algorithms, but bias instability error compensation becomes very critical in long-term navigation applications, so deterministic and stochastic error compensation should be considered together [19]. The main difference between deterministic and stochastic modeling is that in deterministic modelling is that in deterministic modeling one or more inputs must be associated with one or more outputs whereas in stochastic modeling there may be no direct relationship between input and output [25]. However, for low-cost sensors such as MEMS sensors, bias and scale factor errors are quite large, and their repeatability is typically poor due to the dependence on environmental factors, particularly temperature, which makes frequent calibration a necessity [22]. More clearly, the bias and scale factor error values differ due to the operating temperature during the calibration process and during operation [23]. Therefore, there is a need to develop accurate, reliable and efficient thermal models to be used to runtime and non-real time applications. Because these errors accumulate over time, position accuracy degrades if thermal variations and scale factors are not modeled and compensated for both accelerometer and gyroscope bias error [24]. Even if deterministic calibration is performed perfectly, accurate navigation performance cannot be achieved with independent use of inertial sensors, which is unlikely in practice due to repeatability issues [26]. Inertial sensors are typically used with complementary sensors such as GPS [27], laser [29], odometry [30] for this reason. Among the complementary sensors, GPS sensors are the most widely used [31]. The GPS sensor can provide more accurate navigation information, but it is not sufficient on its own due to its low update rate and vulnerable (such as the situation where satellite signals cannot reach) in systems that

require real-time navigation [32]. Especially indoors, the GPS sensor may become inoperable. Therefore, localization systems are used that combine the advantage of the real-time navigation capability of the inertial sensor and the low-frequency GPS sensor navigation accuracy.

The Kalman filter and its variations are frequently used in systems that integrate inertial navigation and GPS sensors [33]. Kalman filter is an iterative set of mathematical equations for estimating the state of a process to minimize the mean of the squared error [16]. Kalman filter has 5 important elements, which are defined as system model, measurement model, state vector, measurement vector and error covariance [17]. The state vector is the parameter calculated by the Kalman filter and cannot be measured directly. The system model describes how the Kalman filter states, and the error covariance matrix change over time. The measurement model specifies the mathematical relationship between the system state and the measurements. The measurement vector contains instantaneous measurement values according to the measurement model. The error covariance matrix indicates the uncertainties in the state estimation and measurements. In order to ensure that the Kalman filter works properly, the errors must be measured and processed to create an error model [12]. The first step of the Kalman filter design used to integrate the GPS sensor and the inertial navigation system is the Q matrix design with the creation of the stochastic error model. The process of characterizing stochastic variation at different temperatures is one of the most important steps in developing a reliable and cost-effective integrated navigation system [8]. The value of the bias and scale factor error differs from the value obtained through the dynamic run-time calibration process (six position test) due to the difference between the runtime sensor temperature and the sensor temperature during calibration [23].

For reliable inertial navigation, the errors of the inertial sensor at various angular velocities at the time of dynamic state must be correlated and modeled with all possible operating temperatures by controlling the temperature of the test environment. In this thesis, a test device that can mechanically reproduce the angular movement of human arms and legs was produced. The device was calibrated at certain angular velocities with the optical reference system. A mobile data acquisition system was developed for the IMU sensor.

3. METHOD

3.1. Determining Motor Type

In the first phase of the design, an analog driven DC electric motor (Robert Bosch BSX 04 372, Germany) was used to form the angular motion. A wooden housing was made to the DC motor (Figure 3.1).

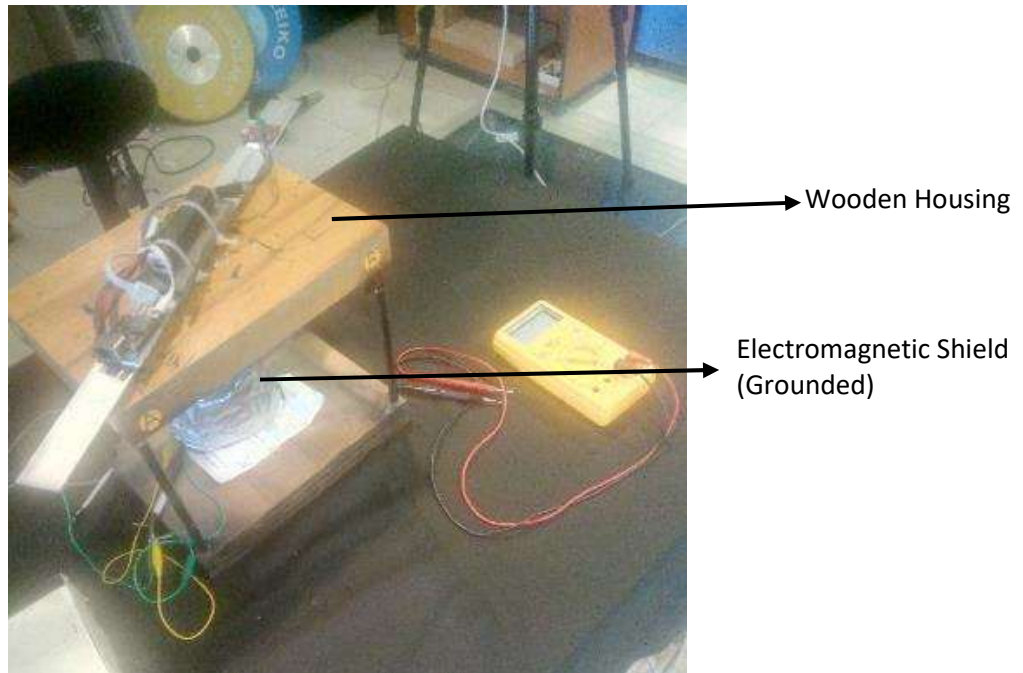


Figure 3.1: General appearance of first test device

Performance tests were performed on the engine using a 3-dimensional motion capture system (Vicon Bonito, United Kingdom) (Figure 3.2).



Figure 3.2 General appearance of test environment

In the test carried out, it was seen that the analog controlled DC motor did not have the desired capability of the brake and start control. Since it is angle controlled, it was decided to use a digitally controlled stepper motor with more advanced control quality and response time.

3.2. Determining IMU Sensor

Data output rate, accuracy and prices of different IMU sensors were compared for the study. Firstly, the MPU9250 (TDK Invesens, United States) sensor with 9 degrees of freedom was examined. The sensor was purchased as a module (Sparkfun Razor M0, United States). The fact that the sensor was well documented and used in many different academic studies was effective in choosing this sensor.

MPU9250 inertial sensor; it consists of the MPU6050 chip, which consists of an accelerometer and gyroscope sensor, and the AK8963 chip, which is a magnetometer sensor. The gyroscope and accelerometer outputs have a 16-bit analog-to-digital converter hardware. The chip has 512 bytes of FIFO memory.

Secondly, a more recent sensor (Bosch Sensortec BMX160, Germany), released in 2018, was examined (Figure 3.3). The BMX160 sensor consists of the BMI160 chip, which consists of accelerometer and gyroscope sensors, and the BMM150 chip, which consists of magnetometer sensor. The BMX160 sensor has 9 degrees of freedom combined with 3 sensors. The gyroscope sensor supports up to 6400 Hz frequency and the accelerometer sensor supports up to 1600 Hz frequency.

Considering the sensor features both, it was seen that the MPU9250 sensor been out of day technologies, and it is recommended not to use this sensor for new designs on the website of the company that produces the sensor.

3.3. Design of Experimental Setup

In the designed electro-mechanical test device, it was decided to use a 2-pole step 1.8 degree Nema 23 model stepper motor to provide rotational motion (Figure 3.3).

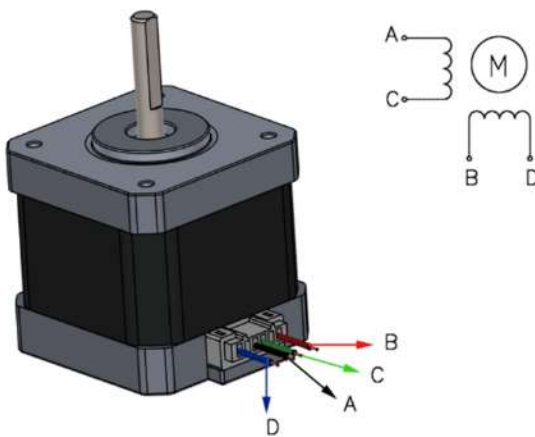


Figure 3.3: Nema23 Step Motor

It was screwed into a wood plate to minimize stepper motor vibrations. In order to minimize the magnetic field effects produced by the motor during operation and not affect

the sensor, the body part of the stepper motor was framed with aluminum material and the material used to framing was grounded (Figure 3.7).

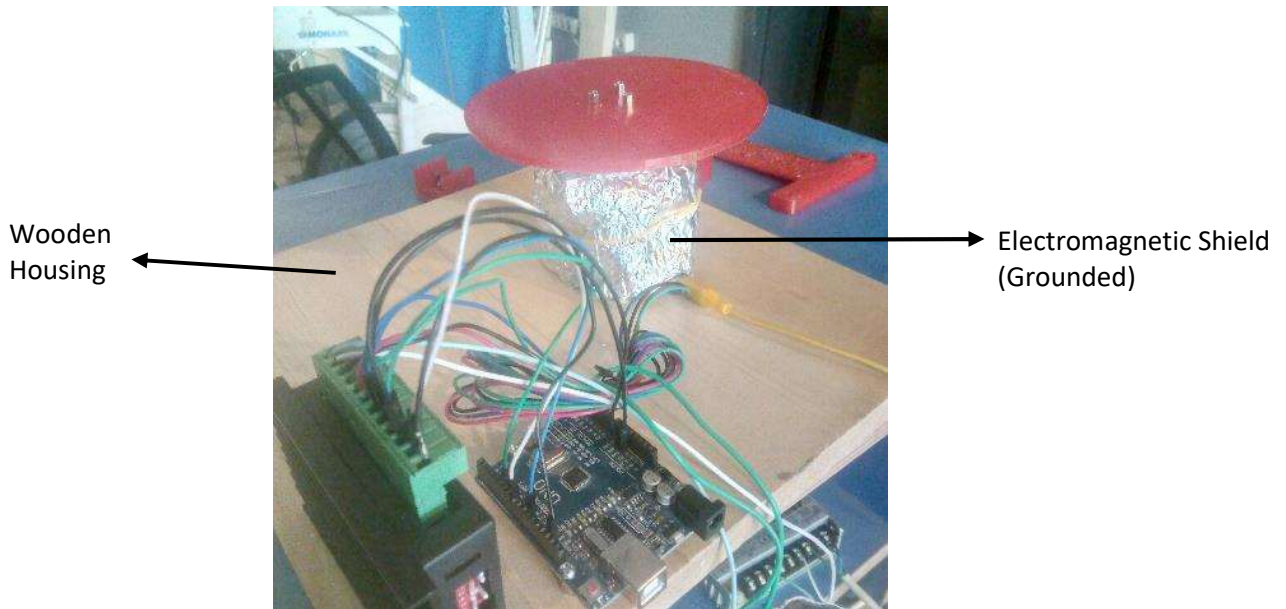


Figure 3.4: General appearance of stepper motor housing

A motor coupler (Pololu, United States) compatible with the 6.35 millimeter shaft diameter of the motor was used (Figure 3.5).

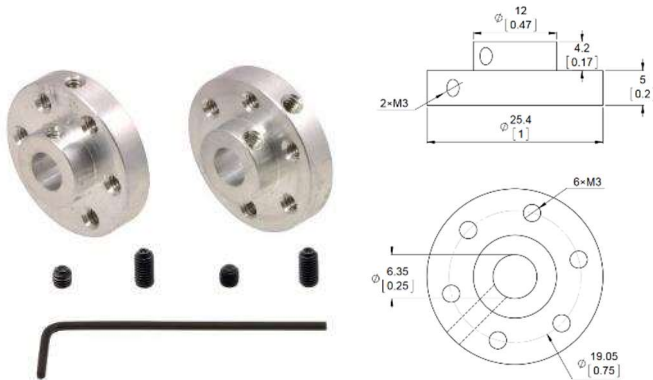


Figure 3.5: Motor coupler

3.3.1. Produced Components

3.3.1.1. Tray Component

A tray component was produced in order to apply the controlled angular movement produced by the stepper motor to the sensor and to fix the sensor at a certain distance from the rotation axis. The tray component was produced using PLA material with 80% fill rate using a 3D printer (Figure 3.6). The tray component has diameter of 280 millimeter.

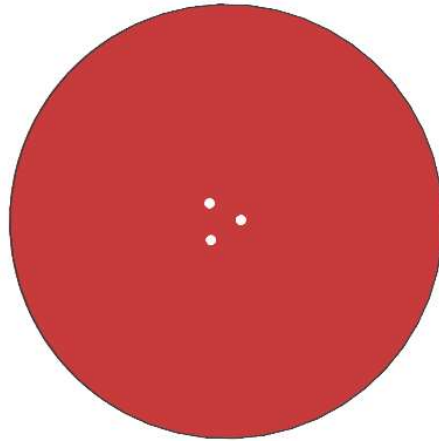


Figure 3.6: Tray component

It was fixed to the coupler with the fixing holes (Figure 3.7)

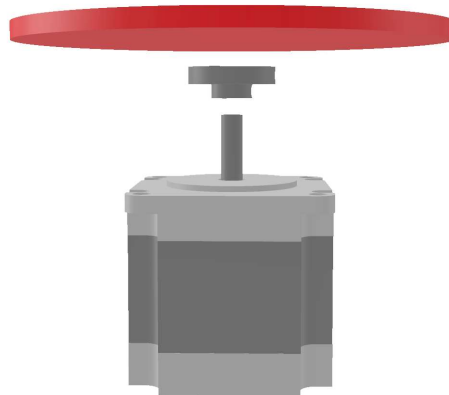


Figure 3.7: Assembling

3.3.1.2. Battery Holder

In order to fix the power battery, which is the heaviest part of the device, exactly perpendicular to the motor rotation axis, a 2-piece design was made (Figure 3.8). Thanks to these parts, the weight of the power battery is fully loaded on the motor shaft, minimizing the effect on the rotation of the test device.

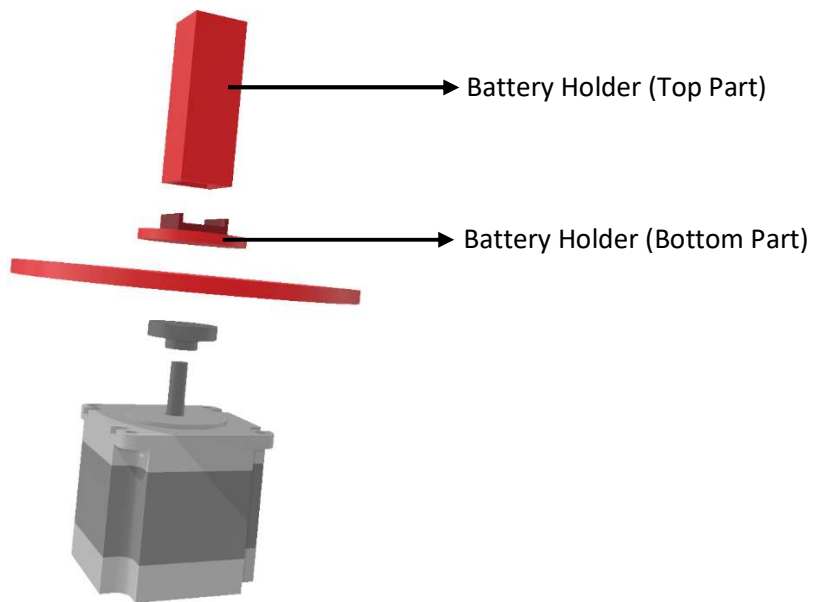


Figure 3.8: Battery Holder

3.3.1.3. Marker Holder

It was produced in order to ensure that the pointer is fixed exactly on the rotation axis for the calibration of the device (Figure 3.9). The component was designed with a diameter of 30 millimeters. Fixing holes in the middle of the component were drilled in accordance with the coupler specified in Section 3.3. A marker capable of reflecting infrared rays with a diameter of 7 millimeters was used.

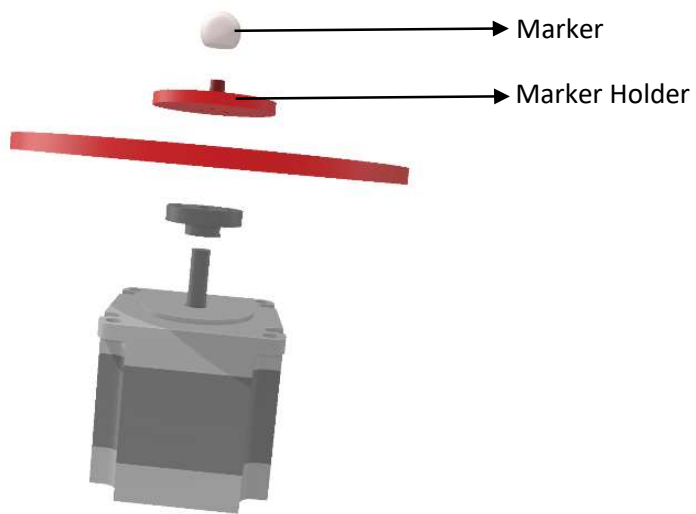


Figure 3.9: Marker Holder

3.3.2. Motor Control System

A driver control card (Toshiba TB6600, Japan) was used to drive the stepper motor (Figure 3.10). The current protection level and step divider value were set using DIP switches located on the driver control card. With the DIP switches, the step number of the stepper motor was divided by 32 and reduced to 0.1125 degrees.



Figure 3.10: Step motor driver

In order to control the stepper motor, the experimental circuit was set (Figure 3.11). The microcontroller software was developed in the C programming language using the AccelStepper [15] library shared by AirSpayce with the GPL license. Speed information in step/second unit and acceleration information in step/second² unit are sent to step motor driver through UART communication.

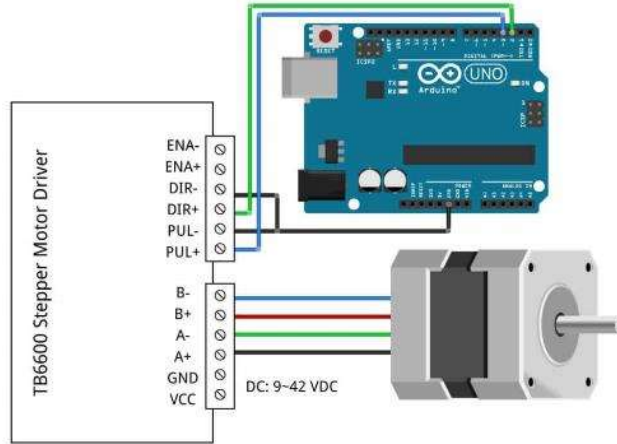


Figure 3.11: Step Motor Control Circuit

3.4. Calibration and Precision Test for Optical System

Sensitivity test was performed to determine the sensitivity of the optical system by using a 5 marker T band (Figure 3.12). At least 3000 samples were collected for each camera.

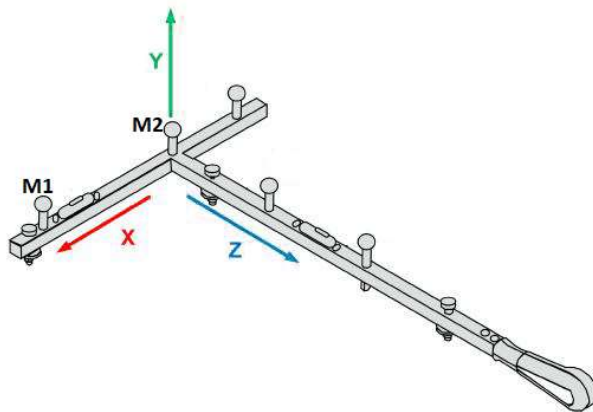


Figure 3.12: 5 Marker T Band

The area of the test environment (indicated with turquoise color) was scanned with 5 marker T Band (Figure 3.13).

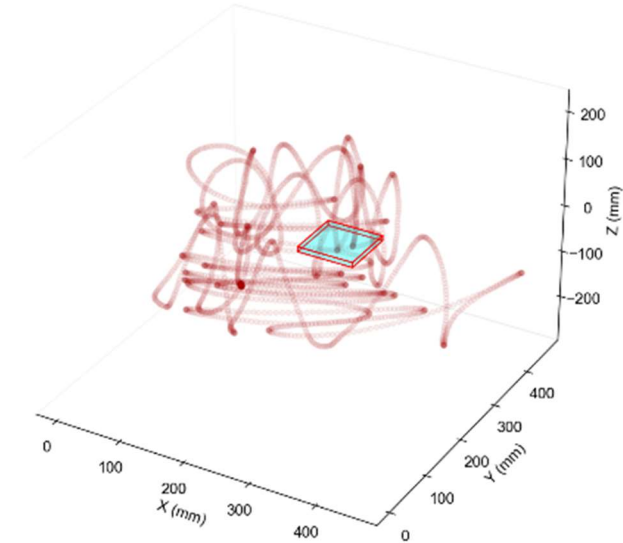


Figure 3.13: Scanned area

The error was calculated by subtracting the length, which is the distance between the two marks measured by optic system, from the actual length, which is the distance between the two marks indicated by T band producer.

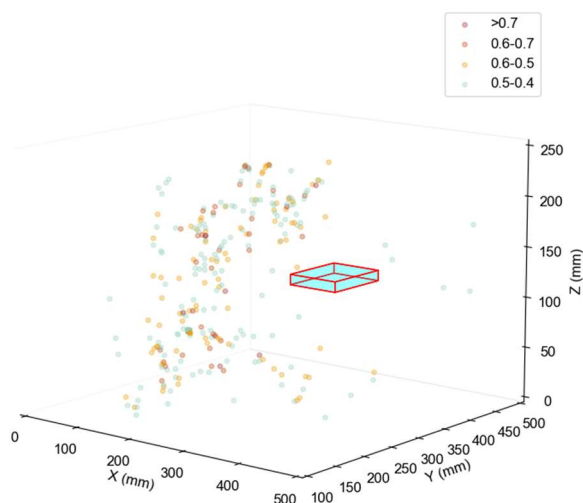


Figure 3.14: Errors up to 0.4 millimeters

The system was found to be reliable in measuring distances of 0.4 millimeters and above. The markers were placed on the tray using fixation component (Figure 3.15). The motor rotating steadily at certain angular velocities was measured with optical camera systems accepted as reference values (Table 3.1).

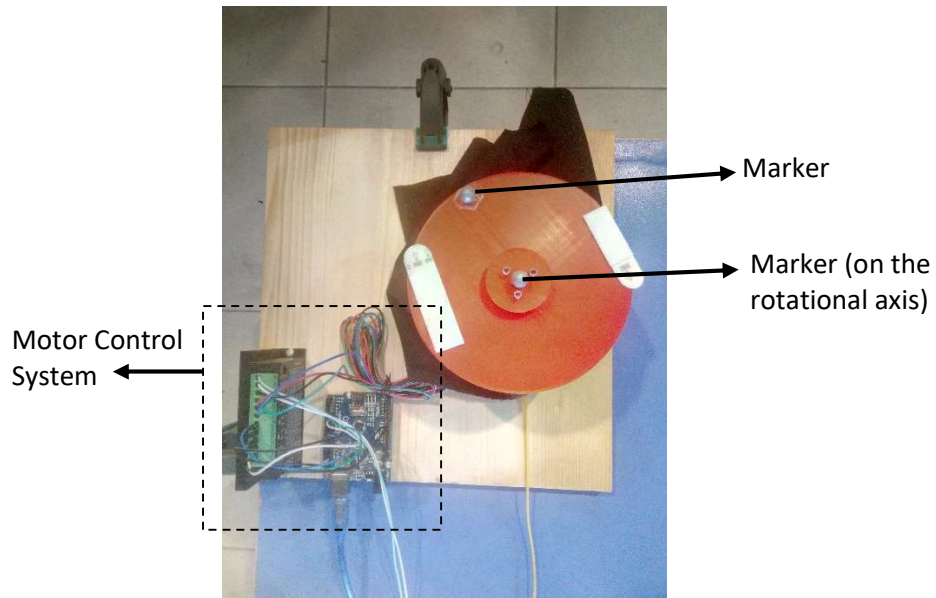


Figure 3.15: Appearance of calibration step

Table 3.1: Calibration results

Applied ($^{\circ}/s$)	Applied (mm)	Measured ($^{\circ}/s$)	Measured (mm)	Error ($^{\circ}/s$)
36	22.618	36.70	23.05	0.70
45	28.273	45.93	28.85	0.93
90	56.547	91.72	57.56	1.72
126	79.165	128.38	80.66	2.38
144	90.475	146.73	92.19	2.73
180	113.094	183.45	115.26	3.45

3.5. Data Acquisition System

3.5.1. Raspberry Pi Configuration

Single board Raspberry Pi Zero 2 (Raspberry pi foundation, United Kingdom) used to acquisition data from IMU sensor. Raspbian OS based on Linux was installed on the board. Default oscillator frequency increased to 900Mhz. Additionally, I2C bus communication frequency updated to 400MHz. All communication with the board was over SSH. Sensor measurement files were transferred using the Samba file sharing software. In this way, data acquisition system has been made completely remotely operable.

3.5.2. IMU Configuration

Sensor sensitivity and data output rates were changed using IMU Sensor registers (Table 3.2).

Table 3.2: Sensor Configurations

Parameter	Register	Default	New Value
Accelerometer PMU	0x03	Suspend	Normal
Gyroscope PMU	0x03	Suspend	Normal
Accelerometer ODR	0x40	100 Hz	800 Hz
Accelerometer RANGE	0x41	$\pm 2G$	$\pm 4G$
Gyroscope ODR	0x42	100 Hz	800 Hz
Gyroscope RANGE	0x43	$\pm 2000^\circ/s$	$\pm 500^\circ/s$

3.5.3. Data Acquisition Software

General flow of the program shown in Figure 3.16.

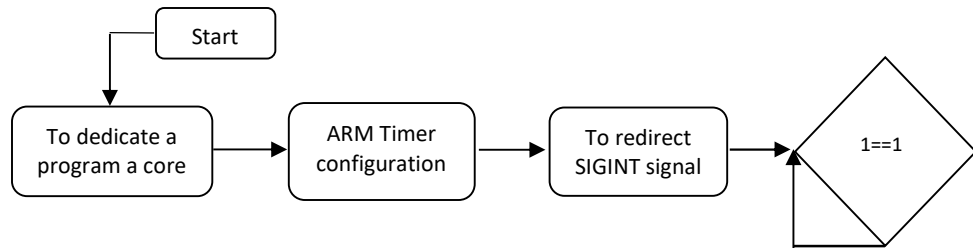


Figure 3.16: General flow of the program

The ARM timer hardware was set to 380 Hz frequency for all experiments. A system call controlled by ARM timer, SIGALRM signal, was redirected to data read function. Read function has read 15 bytes of data from address 0x0C. A system call controlled by user, SIGINT signal, was used to operate the exit procedure of the data acquisition software. The exit procedure writes the data saved in RAM at runtime to the specified file in the SD card memory. Infinite loop defined after configurations made.

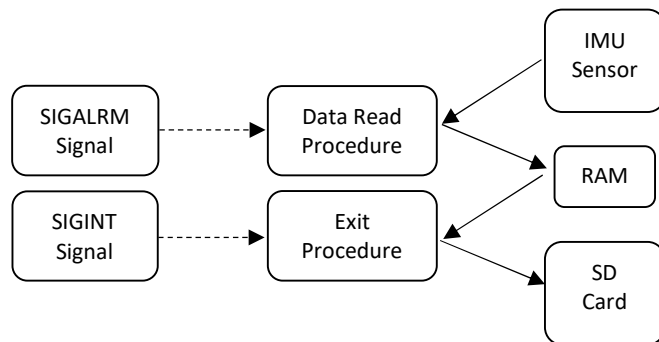


Figure 3.17: Procedures of the program

3.6. IMU Deterministic Error Modelling

Calibration of inertial instruments is necessary to reduce errors. The first step in inertial navigation is to calibrate the deterministic bias, scale factor and misalignment errors of

the inertial sensor [8]. Common methods for calibrating IMUs are primarily designed for in-laboratory testing and high-end sensors such as tactical-grade IMUs. These tests often require the use of special references, such as alignment to a particular frame or special equipment. Six position static testing is among the most widely used [34]. Six position testing requires the inertial system to be mounted on a flattened surface, facing up and down alternately for each measurement axis. There are a total of six positions for an orthogonal sensor trio (Figure 3.19). Six position calibration accuracy depends on how well the axes align with the vertical axes of the local level frame. A perfect cube-shaped mounting frame is required for accurate measurement. In the scope, a plastic frame suitable for the sensor was produced with a 3D printer. A water gage was used to check whether the sensor was in a flat position (Figure 3.18).

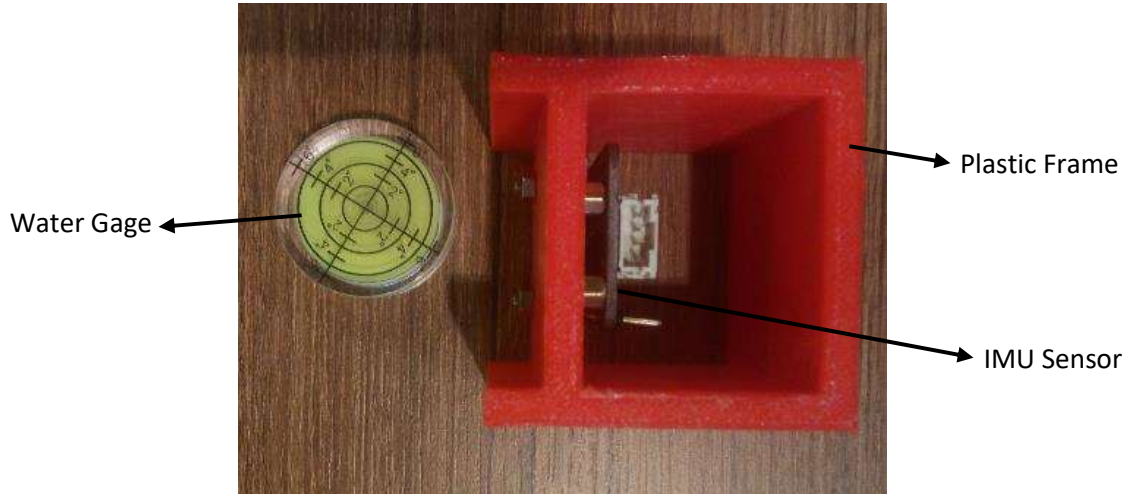


Figure 3.18: Flatness check

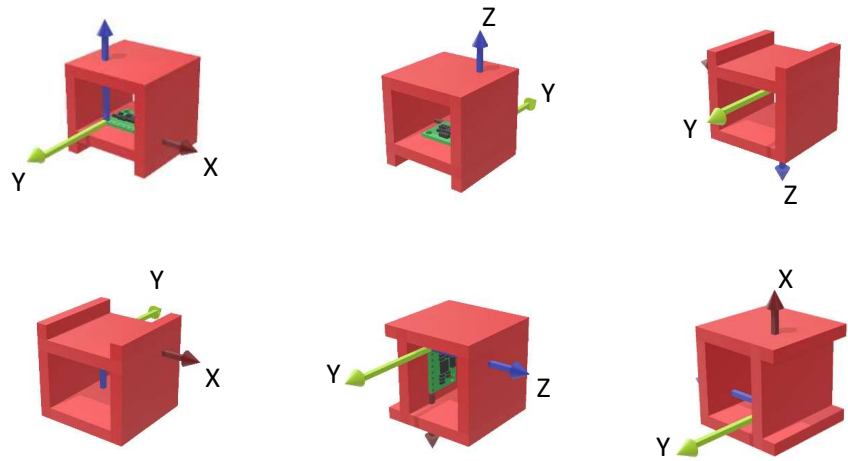


Figure 3.19: Six position experiment

3.6.1. Acceleration and Gyroscope Bias Errors

Six position experiment results and calculated bias errors are shown in Table 3.3 and Table 3.4.

Table 3.3: Six position experiment results

Position	1	2	3	4	5	6
a_x	0.997g	0.006g	-0.002g	-0.999g	-0.007g	-0.000g
a_y	-0.009g	0.998g	0.001g	-0.009g	-0.998g	0.000g
a_z	0.004g	-0.01g	0.008g	0.005g	0.010g	-0.990g

Table 3.4: Calculated Bias Errors

Sensor	X Axis	Y Axis	Z Axis
Accelerometer	-1.247 mg	-0.222 mg	6.671 mg
Gyroscope	1.825 °/hour	1.712 °/hour	2.791 °/hour

In the calculation of gyroscope bias errors, the angular motion of the earth wasn't measured and neglected, since there is no high-precision optical reference IMU sensor in laboratory facilities.

3.6.2. Acceleration Scale Factor and Misalignment Errors

The scale factor error was calculated as proportional to the sensor measuring ranges (Figure 3.19).

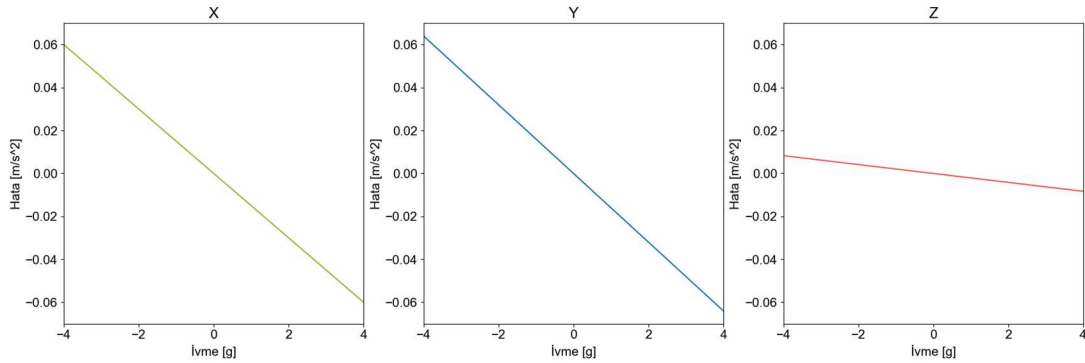


Figure 3.20: Accelerometer Misalignment Errors

Table 3.5: Accelerometer Misalignment and Scale Factor Errors

Scale Factor Error (ppm)	Misalignment Error (degree)
$\begin{bmatrix} 1.55 & 0 & 0 \\ 0 & 1.63 & 0 \\ 0 & 0 & 213 \end{bmatrix}$	$\begin{bmatrix} 0 & 0.46 & -0.02 \\ -0.460 & 0 & 0.048 \\ 0.024 & -0.04 & 0 \end{bmatrix}$

3.7. Angular Movement Experiment Procedures

Experiments were carried out in 45 deg/s and 180 deg/s angular velocities. The experiments were carried out 10 times by moving the sensor angularly for 5 seconds at a constant angular velocity as determined. The angular motion applied to the sensor was intended to simulate the angular movements of the arms and legs during a human's gait (Figure 3.21). Butterworth filter was applied to the measured raw data.

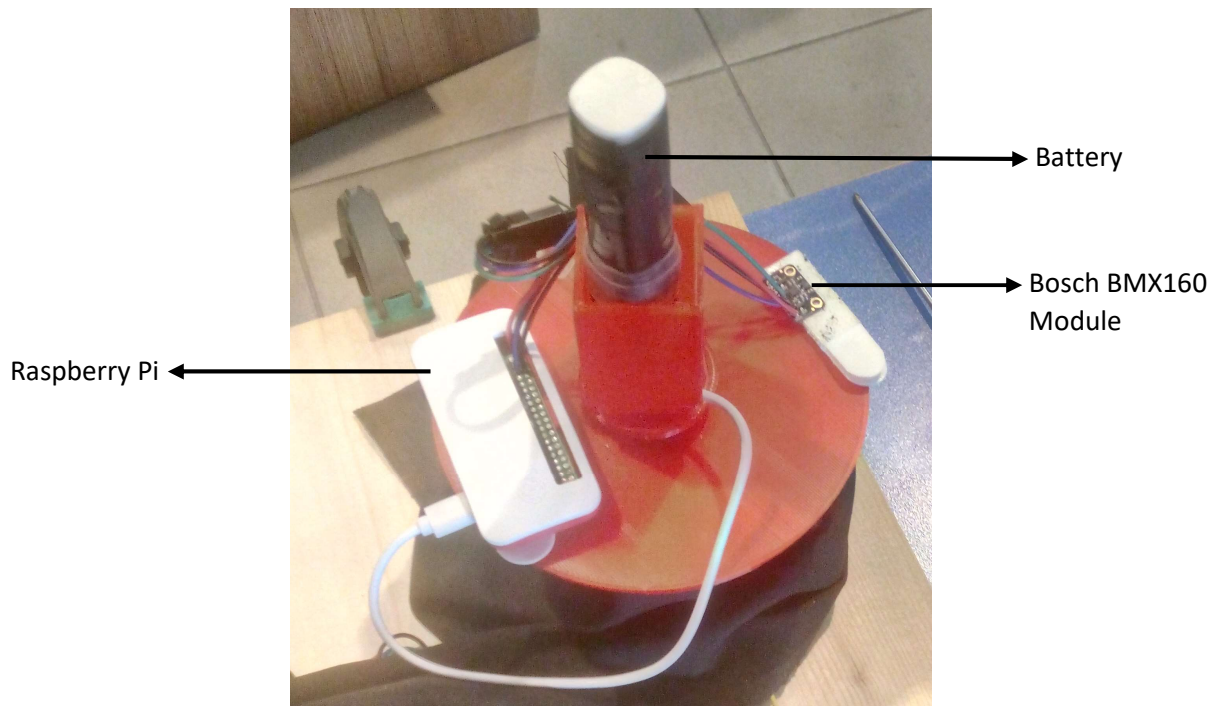


Figure 3.21: General appearance

With the help of the sensor fixing component, the IMU was placed in such a way that the angular movement of the sensor could be applied to the 3 measuring axes separately (Figure 3.22). Sensor temperatures were measured by 24-bit internal temperature sensor.

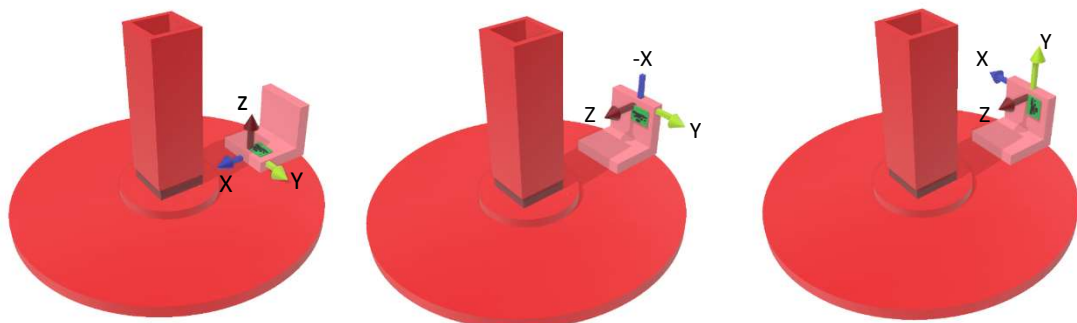


Figure 3.22: Sensor placements

4. FINDINGS

4.1. Device Vibration Findings

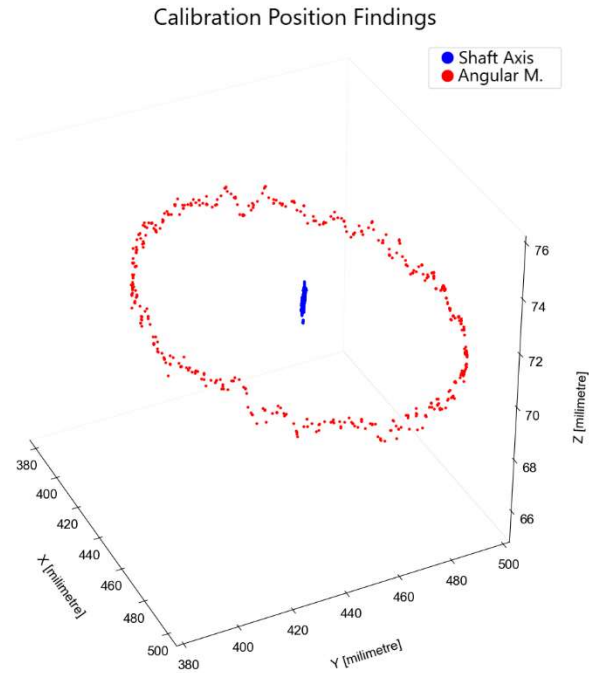


Figure 4.1: Marker positions in device calibration stage

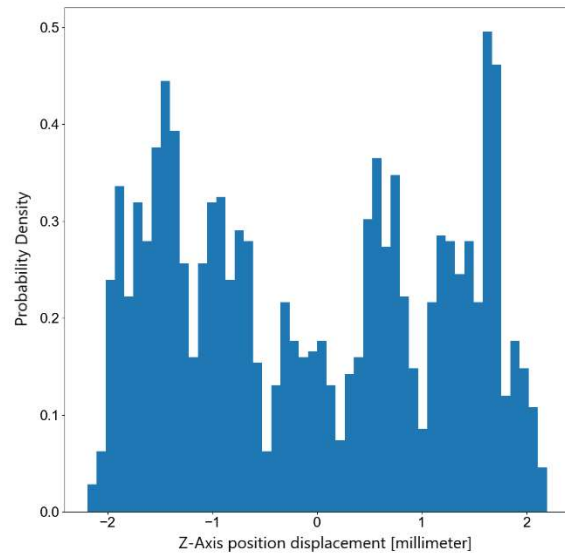


Figure 4.2: Marker Z-axis displacement during calibration

4.2. Sensor Run-Time Temperature Findings

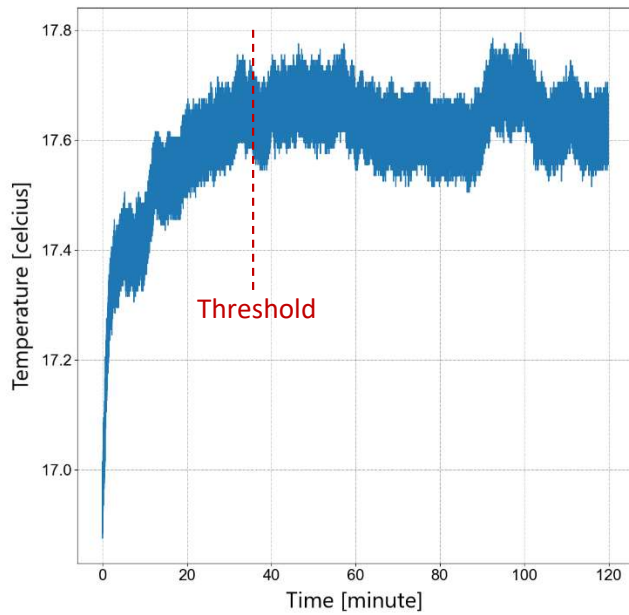


Figure 4.3: Sensor run-time temperature

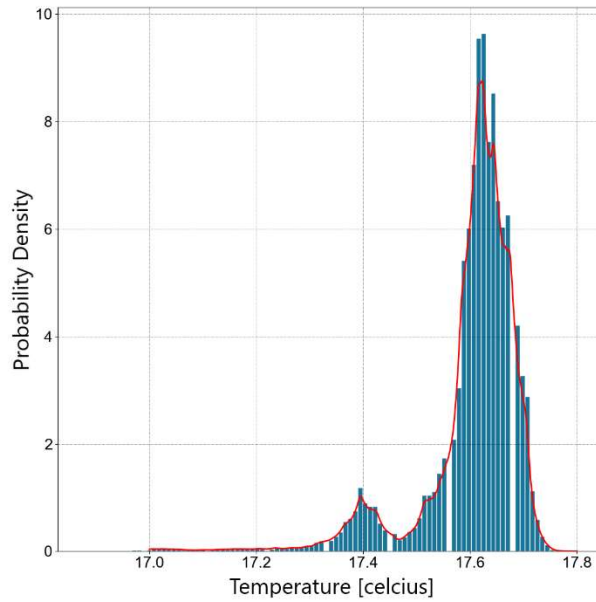


Figure 4.4: Temperature histogram

4.3. 45 degree/second Experiment Findings

4.3.1. Rotation in X-Axis Findings

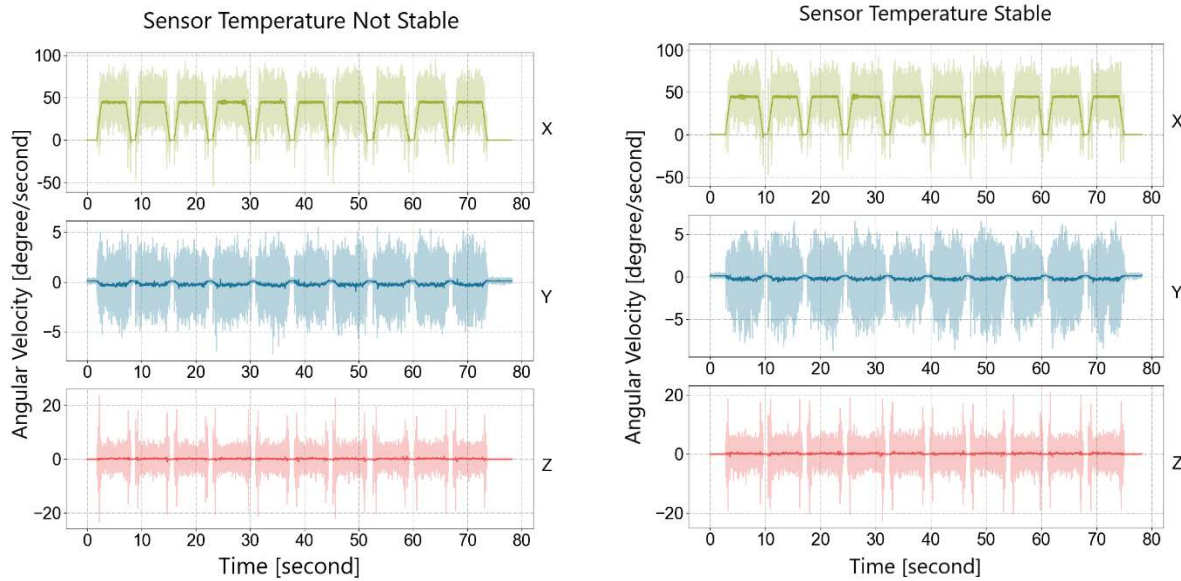


Figure 4.5: 45 d/s X-Axis Raw Findings

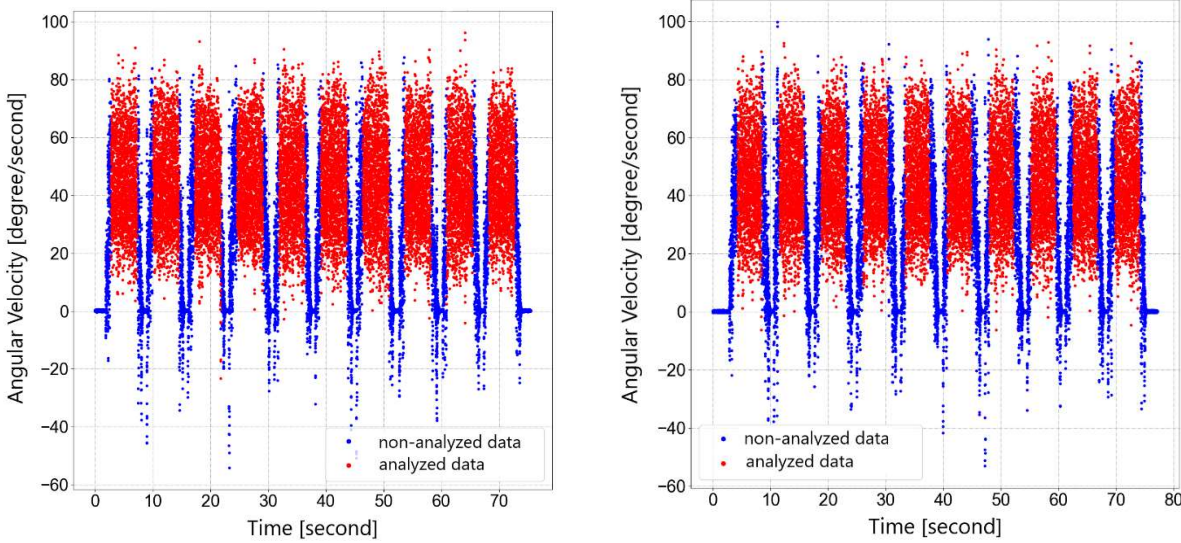


Figure 4.6: 45 d/s X-Axis Data

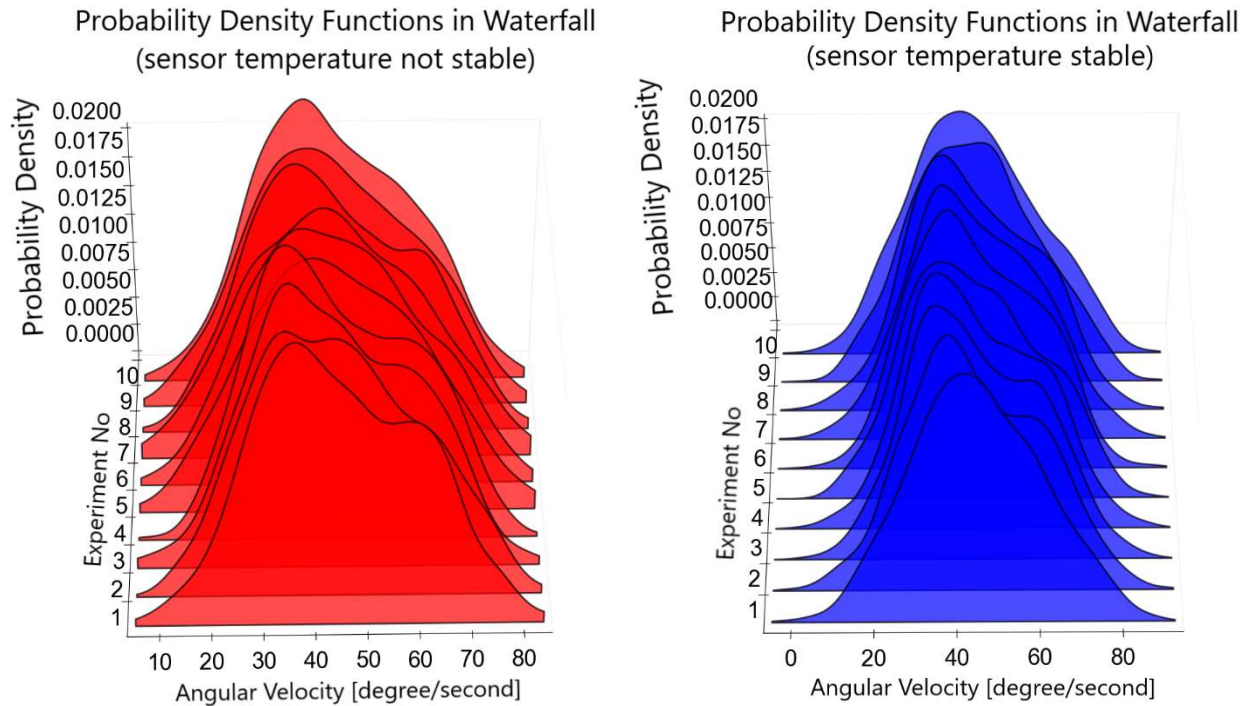


Figure 4.7: 45 d/s X-Axis Probability density function of experiments in waterfall

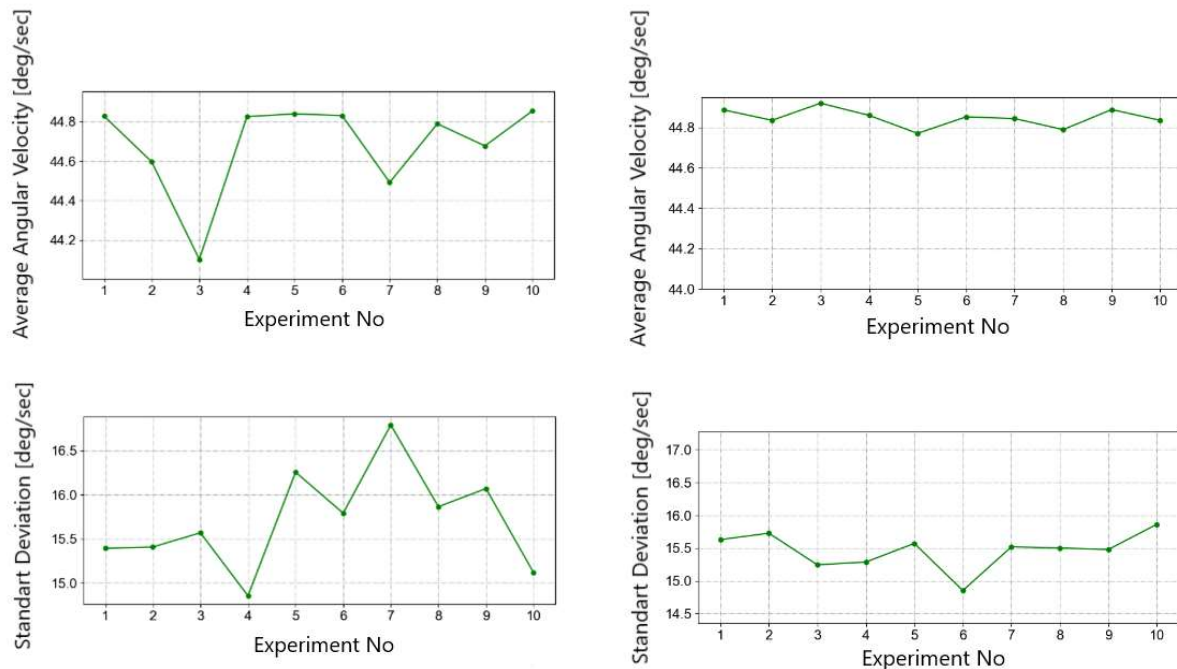


Figure 4.7: 45d/s X-Axis Experiment Analysis Findings

4.3.2. Rotation in Y-Axis Findings

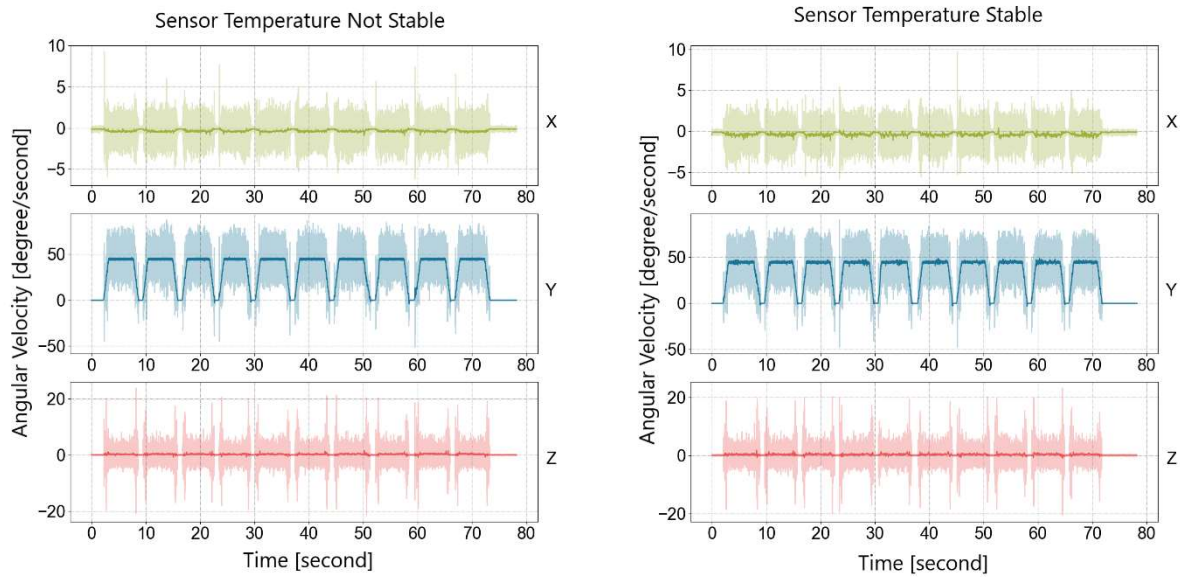


Figure 4.8: 45 d/s Y-Axis Raw Findings

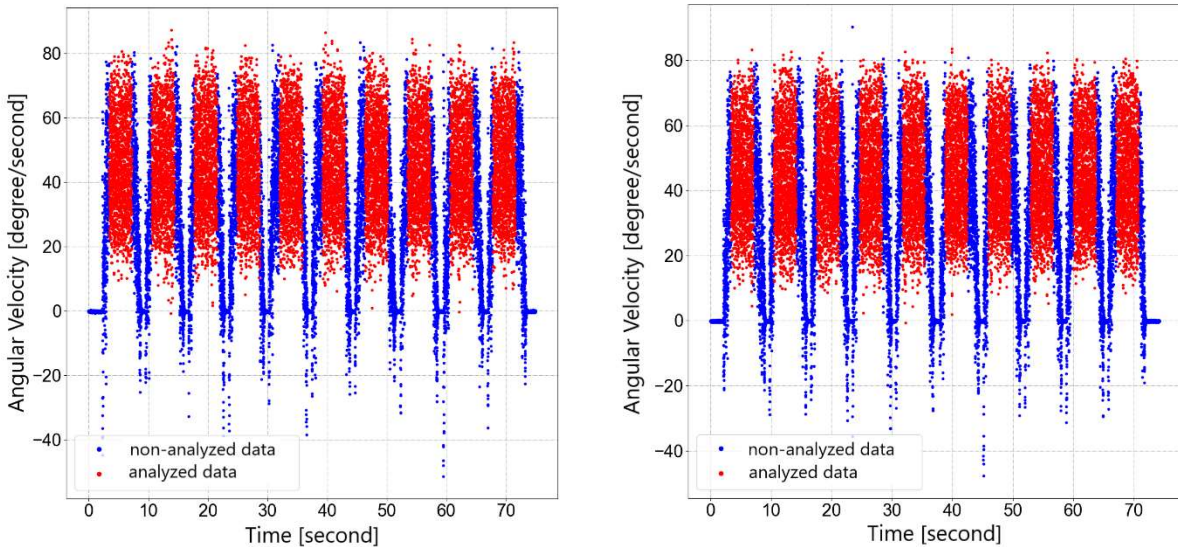


Figure 4.9: 45 d/s Y-Axis Data

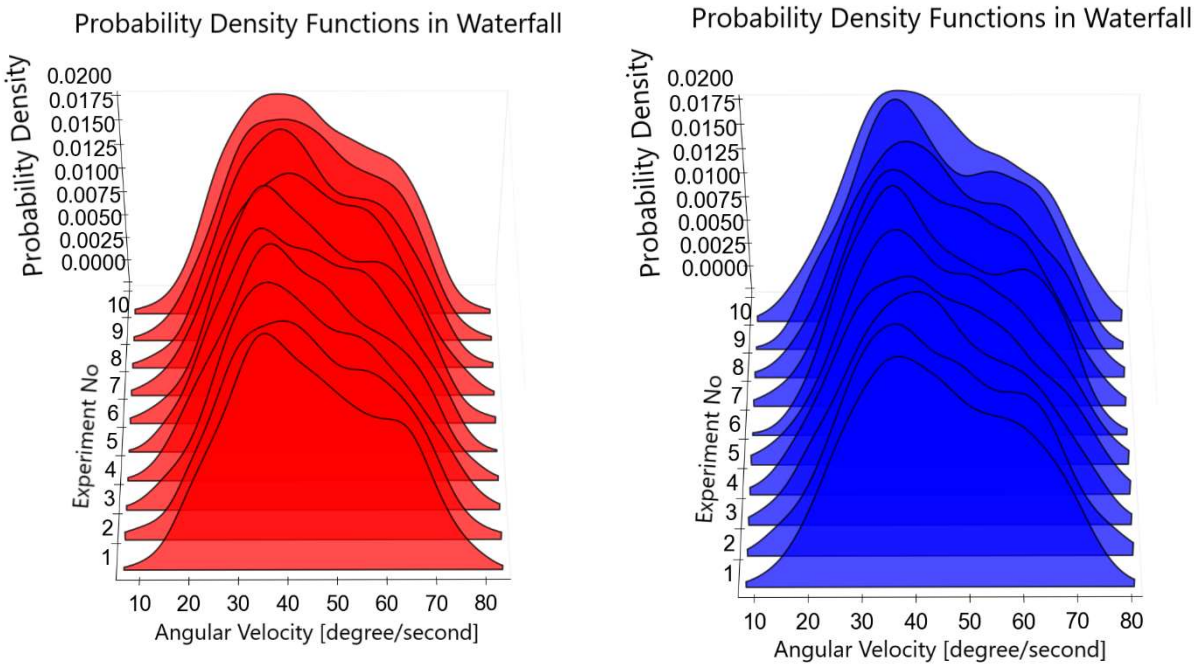


Figure 4.10: 45 d/s Y-Axis Probability density function of experiments in waterfall

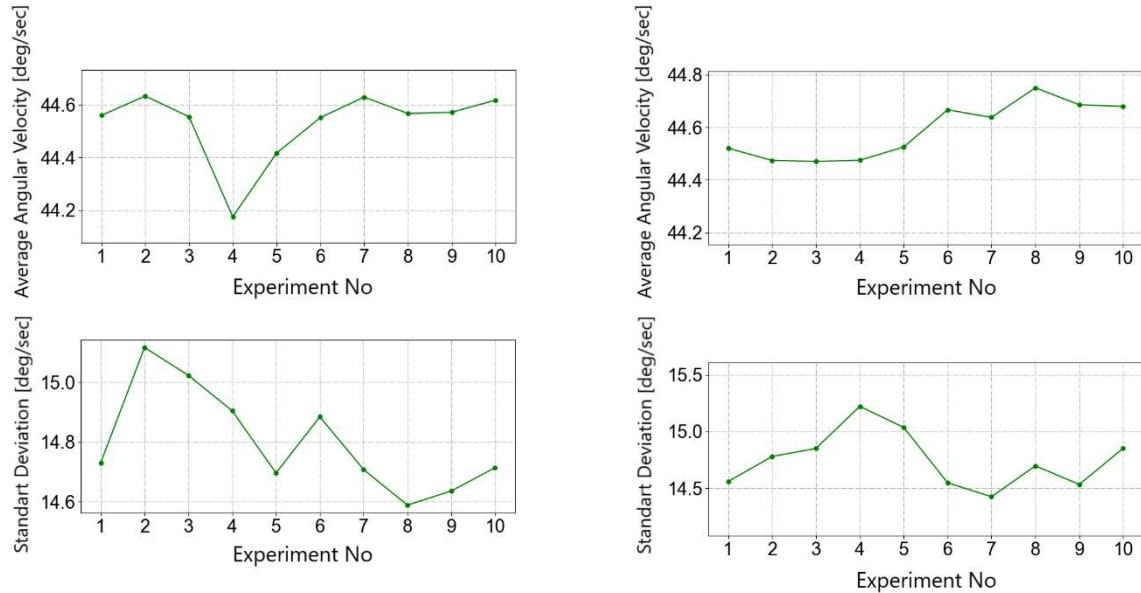


Figure 4.11: 45d/s Y-Axis Experiment Analysis Findings

4.3.3. Rotation in Z-Axis Findings

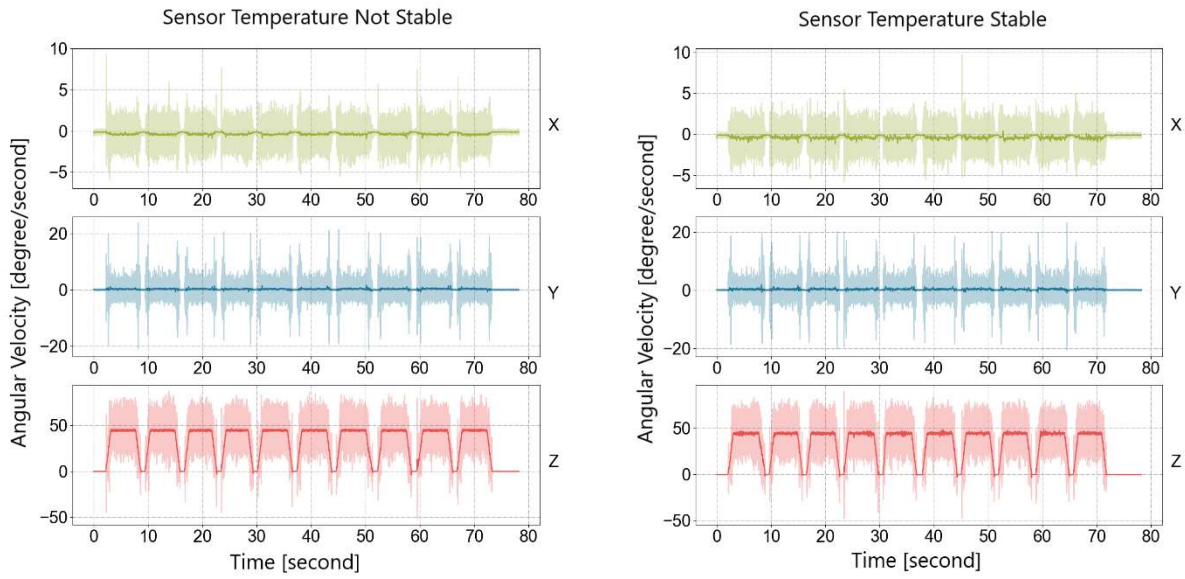


Figure 4.12: 45 d/s Z-Axis Raw Findings

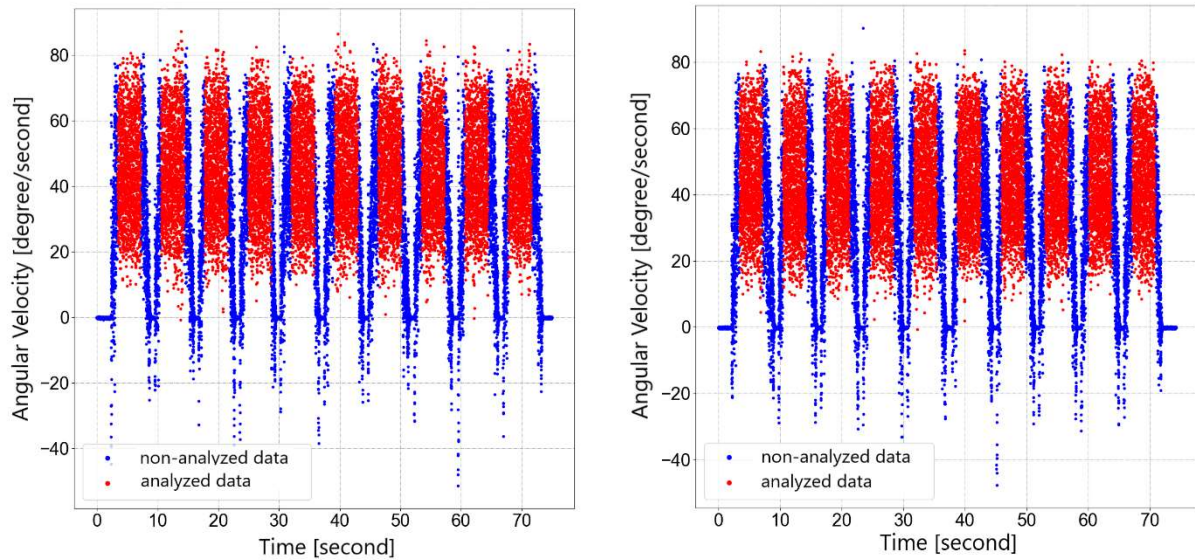


Figure 4.13: 45 d/s Z-Axis Data

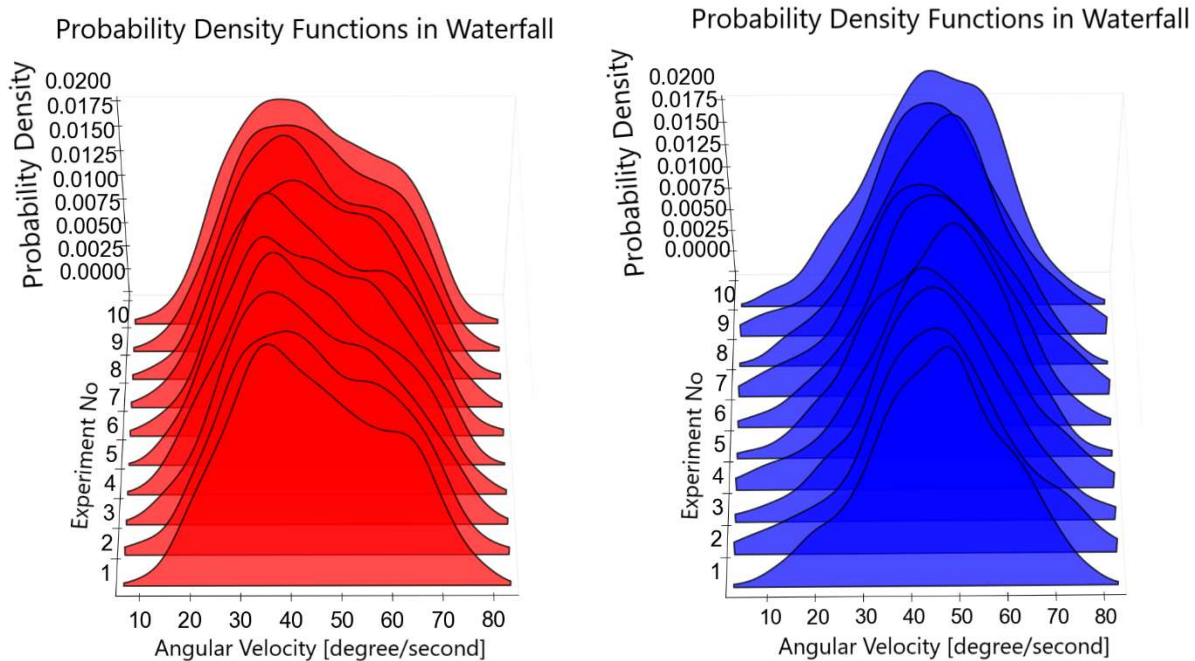


Figure 4.14: 45 d/s Z-Axis Probability density function of experiments in waterfall

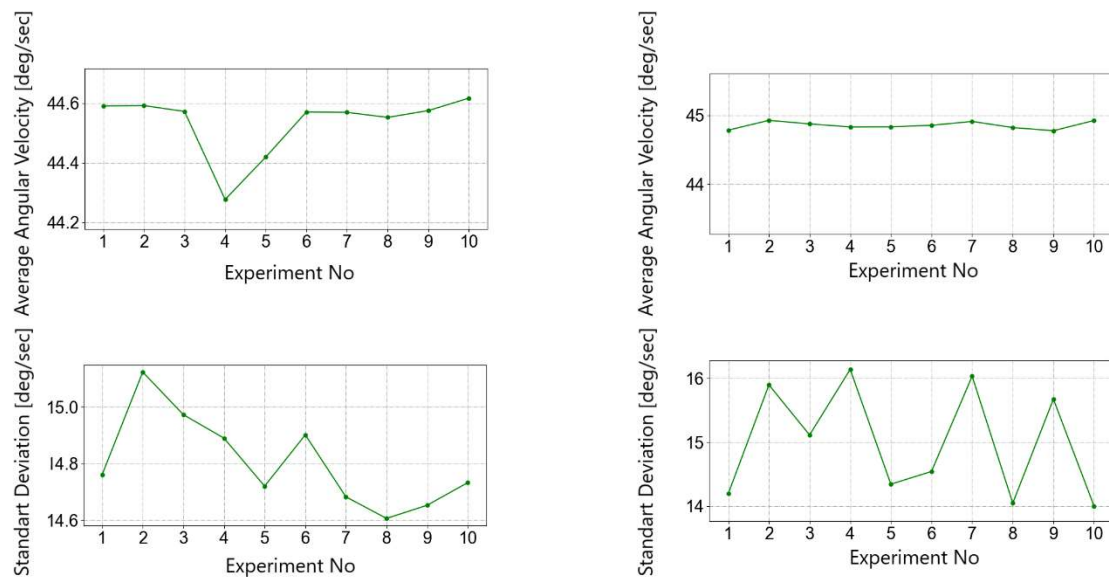


Figure 4.15: 45d/s Z-Axis Experiment Analysis Findings

4.4. 180 degree/second Experiment Findings

4.4.1. Rotation in X-Axis Findings

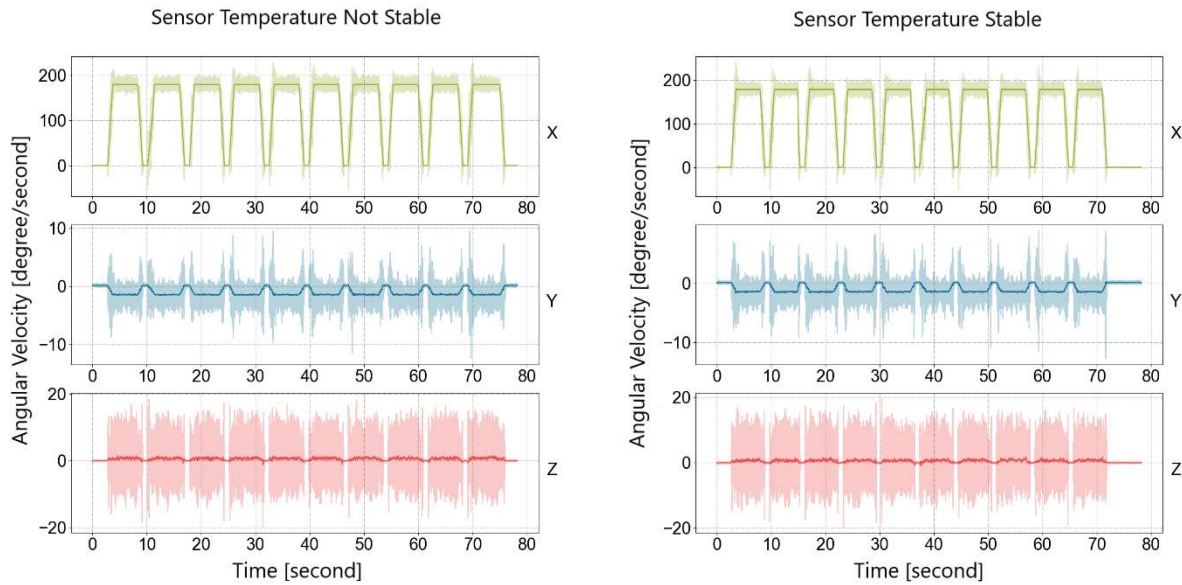


Figure 4.16: 180 d/s X-Axis Raw Findings

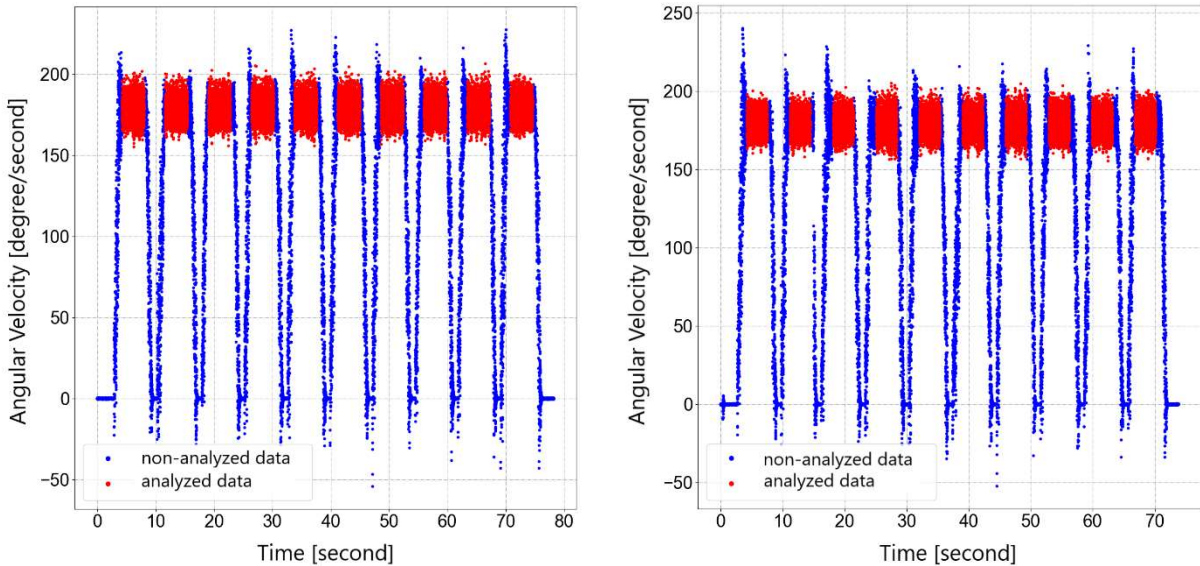
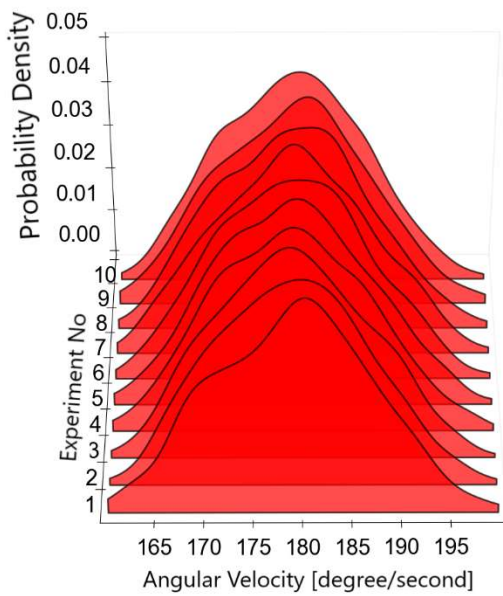


Figure 4.17: Figure 4.13: 180 d/s X-Axis Data

Probability Density Functions in Waterfall



Probability Density Functions in Waterfall

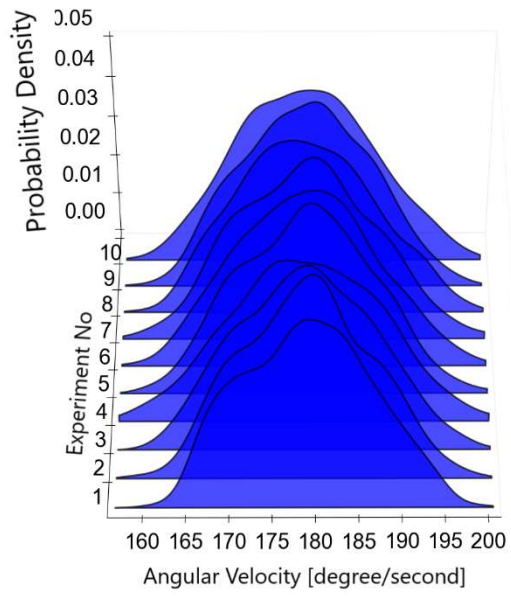


Figure 4.18: 180 d/s X-Axis Probability density function of experiments in waterfall

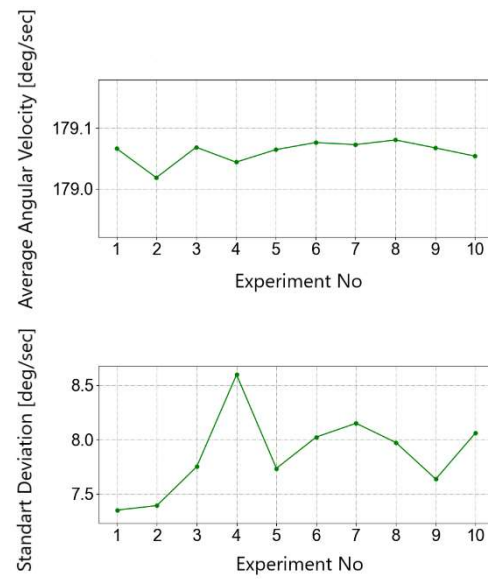
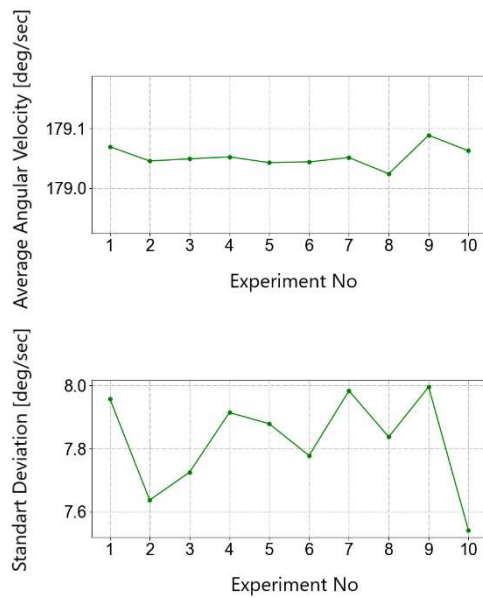


Figure 4.19: 180d/s X-Axis Experiment Analysis Findings

4.4.2. Rotation in Y-Axis Findings

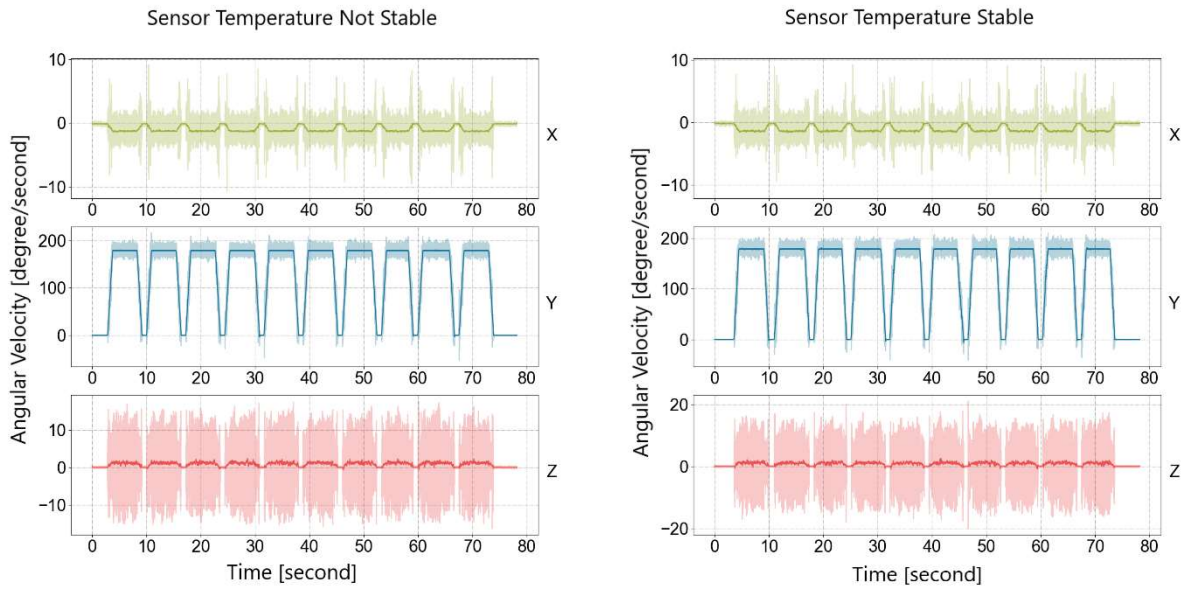


Figure 2.20: 180 d/s Y-Axis Raw Findings

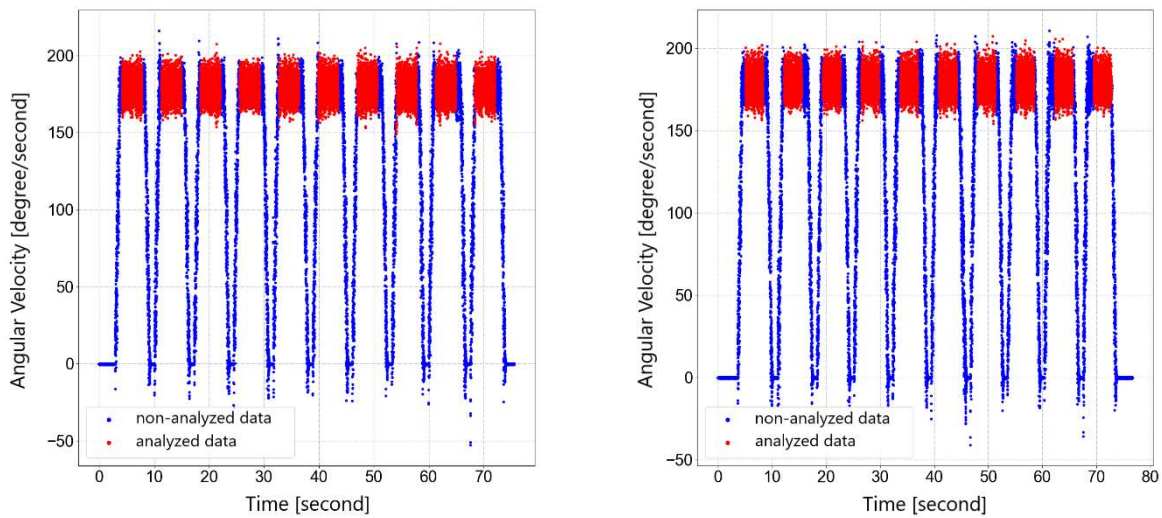
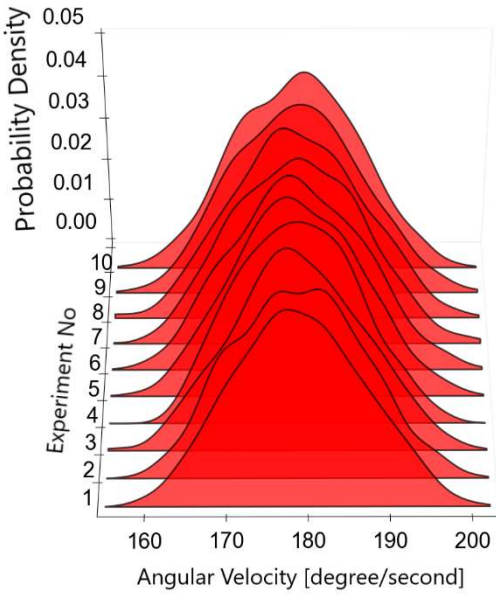


Figure 2.21: 180 d/s Y-Axis Data

Probability Density Functions in Waterfall



Probability Density Functions in Waterfall

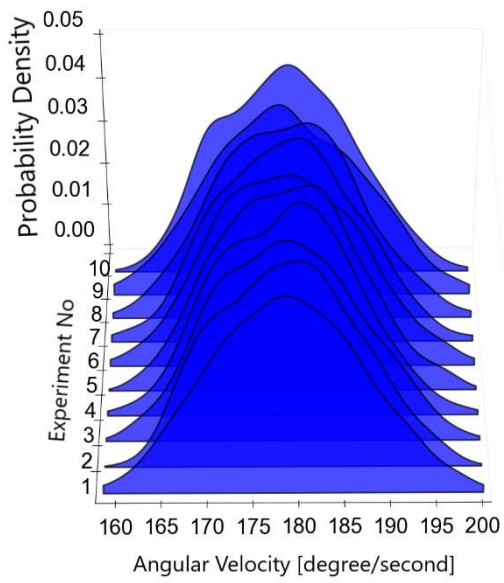


Figure 2.22: 180 d/s Y-Axis Probability density function of experiments in waterfall

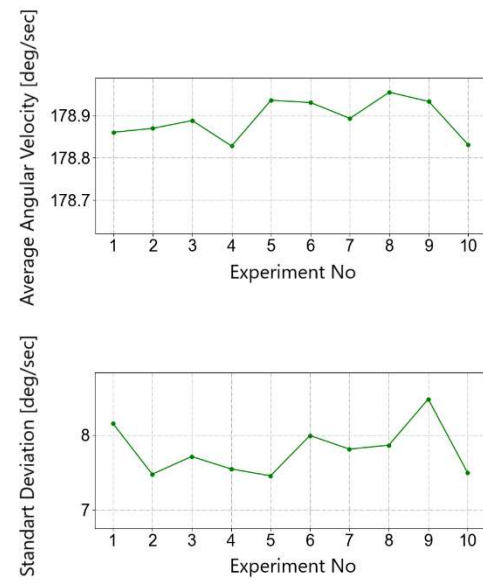
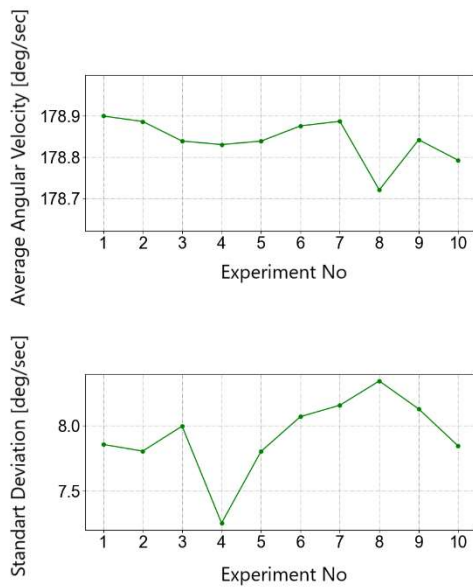


Figure 2.23: 180d/s Y-Axis Experiment Analysis Findings

4.4.3. Rotation in Z-Axis Findings

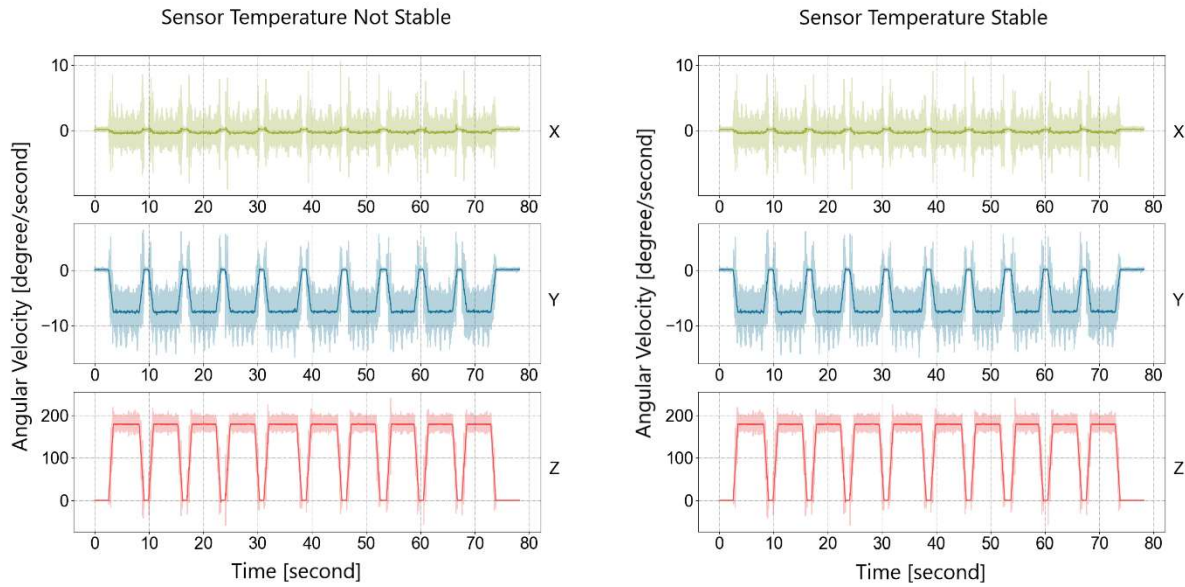


Figure 2.24: 180 d/s Z-Axis Raw Findings

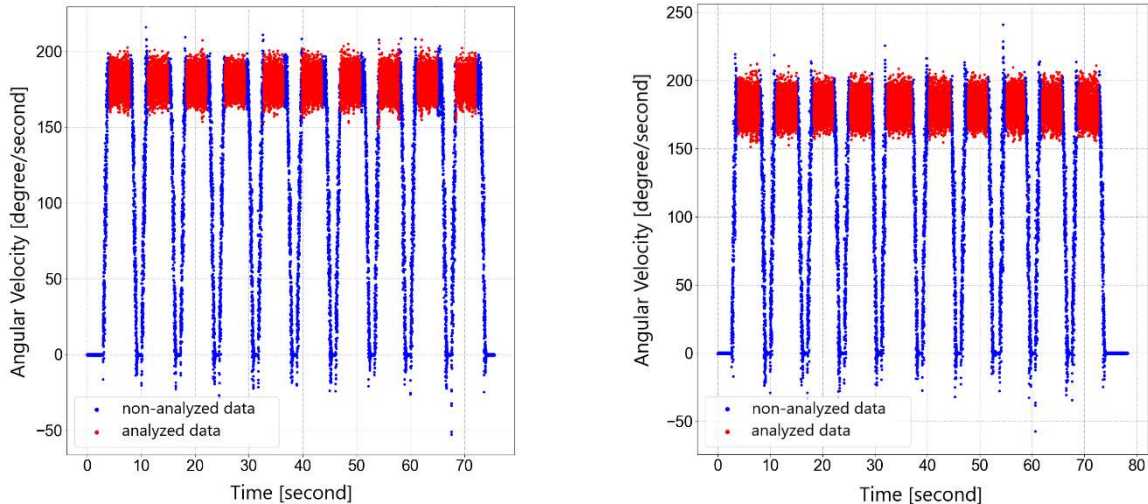
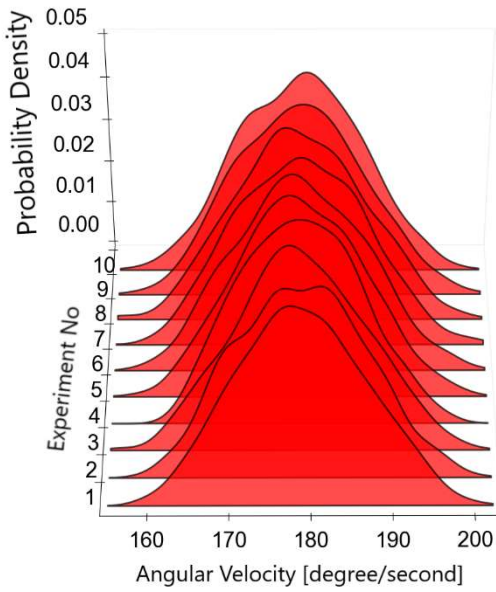


Figure 2.25: 180 d/s Z-Axis Data

Probability Density Functions in Waterfall



Probability Density Functions in Waterfall

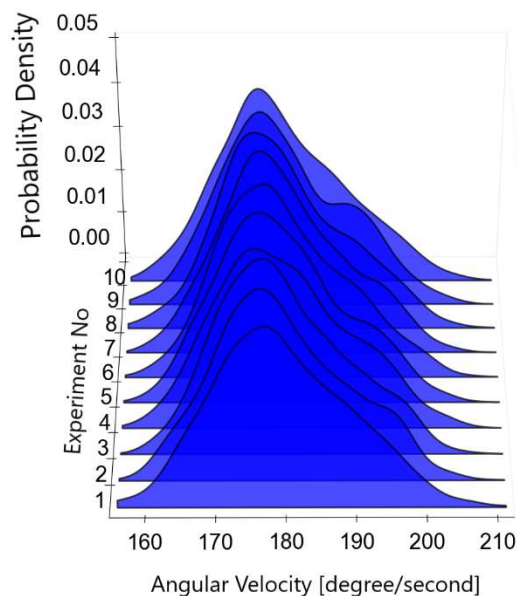


Figure 2.26: 180 d/s Z-Axis Probability density function of experiments in waterfall

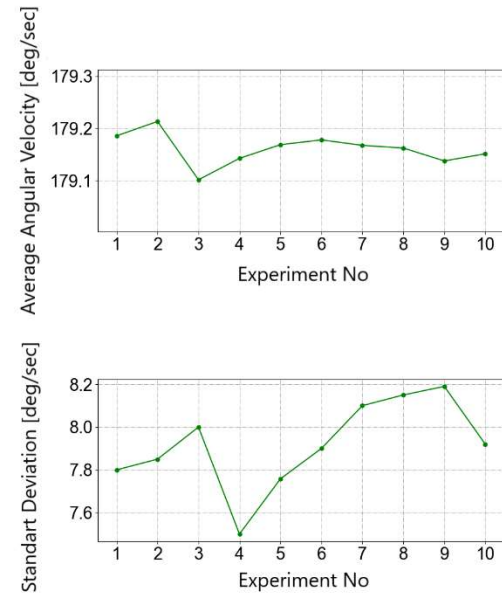
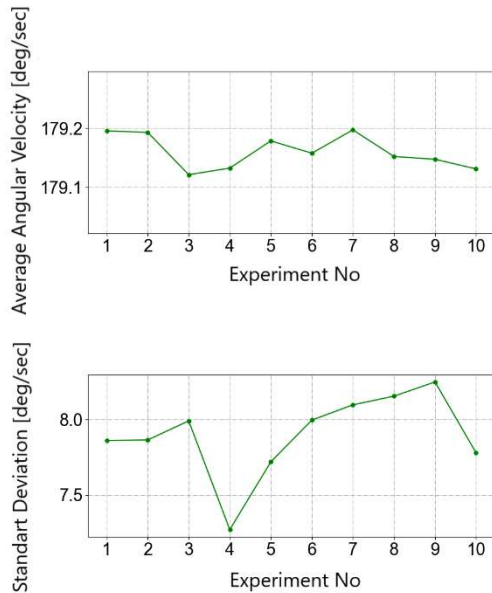


Figure 2.27: 180d/s Z-Axis Experiment Analysis Findings

5. DISCUSSION

It has been found that the sensitivity of the optical system used as the reference is less than 0.4 millimeters and the reference system is reliable enough when the test device is positioned in the middle from the viewing angle of all cameras. In the calibration tests, it was seen that the test device produced vibrations up to 2 millimeters in the Z axis and could not produce the desired 2-dimensional angular movement. It was concluded that the vibration occurred in the experiment is caused by the vibration characteristics of the step motor and it is recommended to use a vibration isolator for shaft in this thesis. In addition, it was determined that the difference between the angular velocity applied to the test device and the angular velocity produced by the motor linearly and the angular velocity sent to the motor as a command increased. It is recommended to use a stepper motor with a higher pole number in this thesis. The temperature parameter, one of the sensor stochastic error sources, was measured for 2 hours with the temperature sensor built into the IMU sensor. When the measurement distributions of sensor temperature were examined, it was seen that there was a temporary condition and then it became stable. In the experiment, it is thought that the obvious temporary situation that occurs when the sensor heats up due to its operation and comes into equilibrium with the ambient temperature is due to the heat permeability of the package material that separates the sensor from the outside environment.

When the raw data of the 45 degree/second angular velocity test applied to the sensor were examined, it was seen that the angular motion formed had significant effects on the other axes. These significant effects are thought to be due to the centrifugal force and the nature of the angular motion. It was observed that the gyroscope measurements varied in a wide range during the time intervals when the angular velocity was fixed and were not stable as desired. It has been understood that the wide range occurred is due to the discrete operation of the stepper motor and the step frequency being much higher than the sensor measurement frequency. When the measurement distributions of the sensor

temperature are examined according to the stability situation, it is seen that the gyroscope errors have less variation and are more stable when the sensor temperature is stable.

In the 180 degree/second angular velocity experiment applied as the second angular velocity, the sensor measurement errors increased approximately 4 times. This high error increase is thought to be due to the high speed than other angular velocity in the experiment. It has been observed that the error difference between the temperature stable state and the temperature non-stable state is close due to the fact that the error has grown so much, and the skidding masks this situation. When the sensor data (analyzed data) is examined for 180 degree/second angular velocity, a change in a narrower range was observed at the angular speed of the measurements at 45 degree/second compared to the experiment. It is because higher angular speed is applied to the motor, making the movement more analog with the frequency of the movement steps.

6.RESULTS

1. Step motors are suitable for a low-budget test device that can simulate human arm and leg angular movements in terms of control capability after the necessary conditions are met.
2. The sensor temperature becomes stable within an average of 30 minutes at a temperature of 17°C, and it becomes more stable in terms of temperature-related gyroscope errors.
3. It is recommended to connect a gearbox (reducer) to the motor shaft in order to reduce the step angle of the step motor below the measurement sensitivity of the sensor, and to prefer step motors with higher pole number, as it will make more analogous.
4. A sensor chip should be chosen where sensor measurements can be read in analog and digitization errors should be reduced by using a higher resolution analog to digital converter.
5. Using the temperature experimental setup with thermal chamber should be created and a temperature dependent error model should be calculated.